Electronic Supplementary Material (ESI) for Dalton Transactions.
This journal is © The Royal Society of Chemistry 2024

Supporting Information for

Non-coordinating Counteranion as a Powerful Tool to Tune the Activity of Copper Water Oxidation Catalysts

*Xin Li, Lijuan Wang, Mengjiao Shao, Xueling Song and Lei Wang**

School of Materials and Chemistry, University of Shanghai for Science and Technology, Shanghai 200093, China

Table of Contents

Experimental Methods

Synthetic Methods and Materials. All ligands, salts, other reagents and solvents were purchased from commercial sources and used as received.

Synthetic procedures. The catalysts in this study were prepared according to the literature (as shown in **Figure S1**)[1]. The Cu complexes, $[Cu(bpy\text{-}R)(OH)_2](OAc)_2$ were synthesized by mixing 4 mmol 2,2'-bipyridyl derivatives and 4 mmol $Cu(OAc)_2$, and stirred in 30 mL methanol for 9 h. Then the solution was concentrated to ~5 mL and filter it to give rise to the blueish solid, which was further dried under vacuum at 50 ^oC for 4 hours, as the final product. All three salts were characterized by mass spectrometry. Electrospray ionization mass spectrometry (ESI-MS) was performed with a Thermo ScientificTM Q ExactiveTM Mass Spectrometer using methanol as the eluent (**Figure S2-S3**, Supporting Information). In methanol, the complexes are in dimer states, $[(bpy\text{-}R)Cu(\mu\text{-}OH)]_2$, which are consistent with previous conclusions[1-3]. Elemental Analysis (calcd., found for $C_{10}H_{10}CuN_2O_2 \cdot 2CH_3COO^-$): C (45.22, 46.83), H (4.34, 4.39), N (7.53, 7.85). Elemental Analysis (calcd., found for $C_{16}H_{20}CuN_2O_6 \cdot 2CH_3COO^-$): C (48.06, 47.42), H (5.04, 5.09), N (7.01, 7.00).

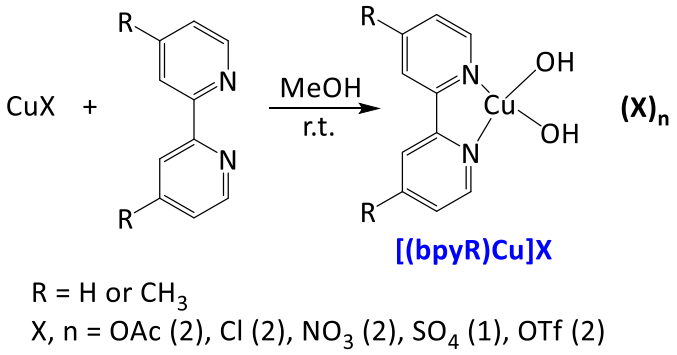

Figure S1. Synthesis procedures for catalysts in this study. **Note:** to simplify the name, all complexes were denoted as [(bpyR)Cu]X.

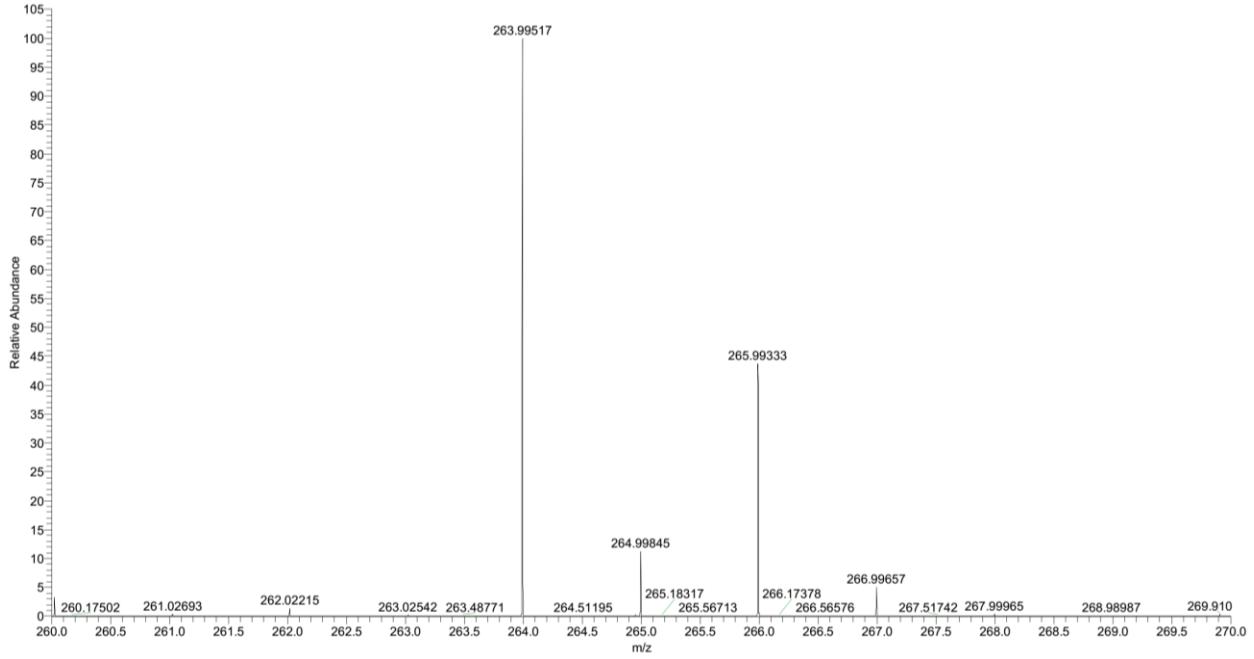

Figure S2. Representative mass spectrum for [(bpyH)Cu]X.

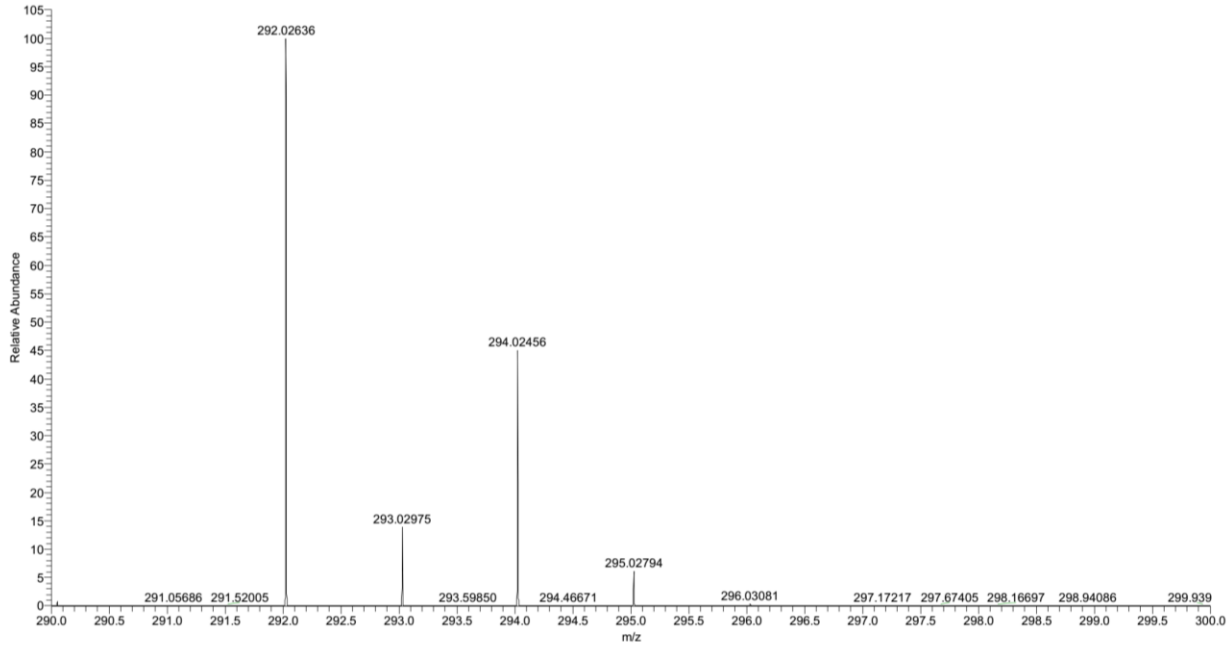

Figure S3. Representative mass spectrum for [(bpyCH$_3$)Cu]X.

Physical Methods

Reported pH values were measured on a REXE-301F pH Metera glass electrode after calibration with standard buffer solutions. Infrared spectroscopy was measured with a Perkin Elmer's SPE CTRUM 100 Fourier Transform Infrared Spectrometer. Electronic absorption spectra were recorded with a UV-visible Shimadzu-2700i diode-array spectrophotometer and were corrected for the background spectrum of the solvent. The molar extinction coefficients, ε ($M^{-1}cm^{-1}$), were calculated by the Beer-Lambert Law: ε =A/(cl), where the concentration, c, is measured in mol dm^{-3} (M^{-1}) and the cell path length, l, in cm. Unless otherwise noted, cyclic voltammograms (CVs) and square wave voltammograms (SWVs) were measured with a CH Instruments CHI-760E bi-potentiostat at ambient temperature (21-24 °C) in a single compartment cell with a 3.0 mm glassy carbon disc working electrode, platinum wire counter electrode, and Ag/AgCl (3 M KCl) reference electrode[4]. The reference electrode was calibrated with the $[Fe(CN)_6]^{3-}$/ $[Fe(CN)_6]^{4-}$ couple[5]. Electrochemical data were calibrated with respect to the NHE by incorporating a voltage shift of 0.199 V to the recorded potential measurements. All potentials are expressed in relation to NHE, unless explicitly indicated otherwise. Solutions contained 1 mM analyte in aqueous solution containing 0.1 M buffer solutions. The buffer solution was prepared by initially combining 0.1 M NaOH and 0.1 M NaOAc solutions, followed by precise pH adjustment using the respective acid or base to achieve the desired pH. The CPE experiments were carried out at a potential of 1.4 V for [(bpyH)Cu]X and 1.5 V for [(bpyCH_3)Cu]X versus NHE reference electrode, using a glassy carbon electrode in a 0.1 M NaOAc/NaOH solution at pH = 12.5. Gas Chromatograph (GC) is measured by Techcomp GC 7980.

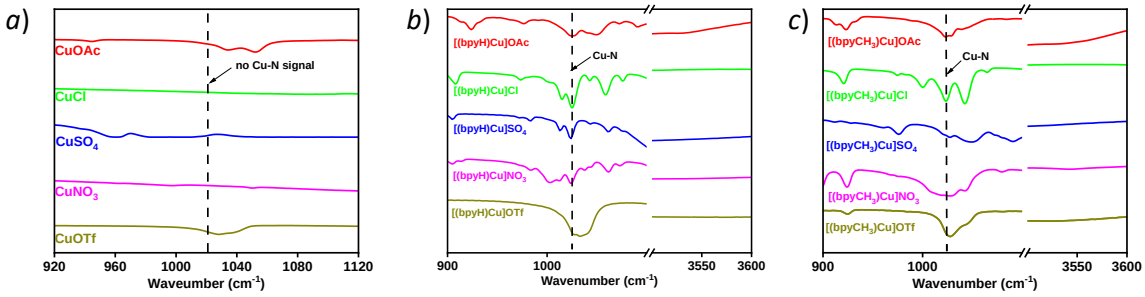

Figure S4. IR spectrum of a) the CuX, b) the [(bpyH)Cu]X, and c) the [(bpyCH$_3$)Cu]X powder.

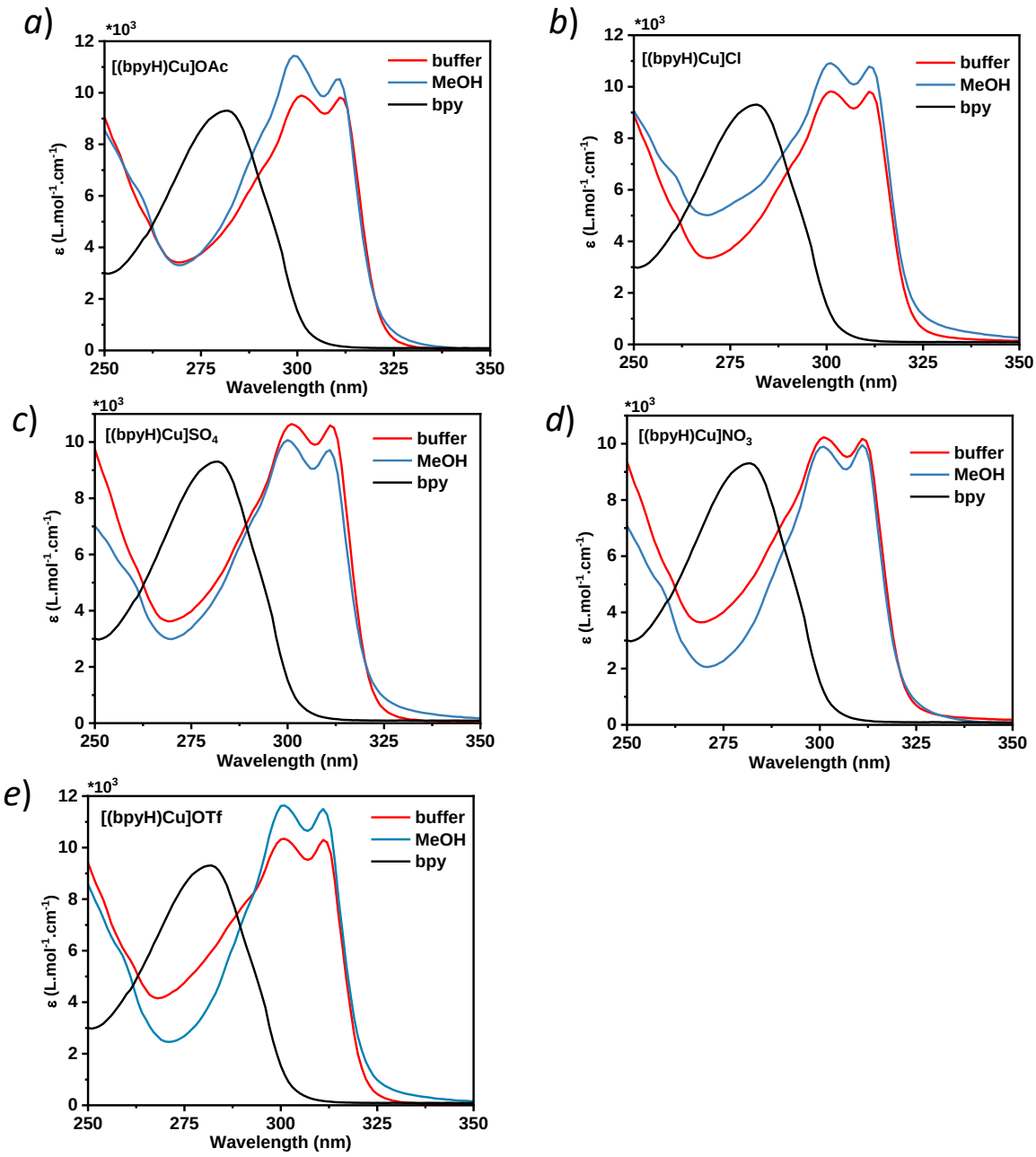

Figure S5. UV-Vis spectrum of 2,2'-bipyridine in methanol, [(bpyH)Cu]X in methanol, and 0.1M pH 12.5 NaOH/NaOAc buffer solution.

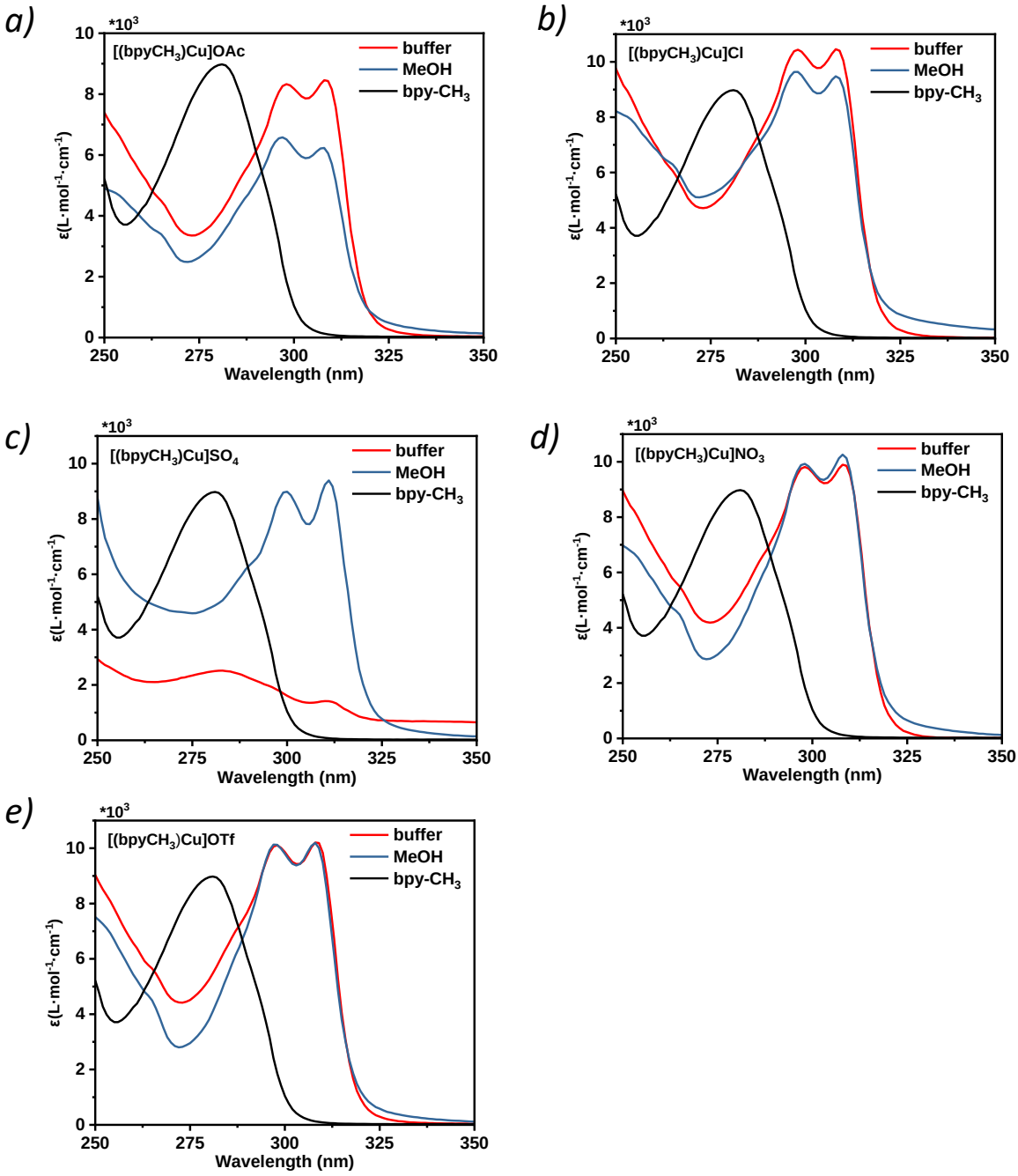

Figure S6. UV-Vis spectrum of 4,4'-dimethy-2,2'-bipyridine in methanol, [(bpyCH$_3$)Cu]X in methanol and 0.1M pH 12.5 NaOH/NaOAc buffer solution.

Table S1. Summary for UV-Vis properties of 0.1 mM copper complexes and IR spectrum.

Catalyst	UV-Vis in pH 12.5 buffer (nm)	UV-Vis in MeOH (nm)	IR (cm^{-1})
[(bpyH)Cu]OAc	301 311	298 307	1024 (Cu-N) 3138~3575 (O-H)
[(bpyH)Cu]Cl	301 311	301 310	1025 (Cu-N) 3020~3122 (O-H)
[(bpyH)Cu]SO_4	301 311	300 311	1020 (Cu-N) 3008~3122 (O-H)
[(bpyH)Cu]NO_3	301 311	301 311	1024 (Cu-N) 3012~3128 (O-H)
[(bpyH)Cu]OTf	301 311	301 311	1029 (Cu-N) 3059~3310(O-H)
[(bpyCH_3)Cu]OAc	296 307	296 307	1023 (Cu-N) 3136~3650 (O-H)
[(bpyCH_3)Cu]Cl	298 307	298 307	1023 (Cu-N) 3124~3651 (O-H)
[(bpyCH_3)Cu]SO_4	/	300 311	1026 (Cu-N) 3129~3627 (O-H)
[(bpyCH_3)Cu]NO_3	298 307	298 307	1019 (Cu-N) 3277~3671 (O-H)
[(bpyCH_3)Cu]OTf	298 308	298 308	1026 (Cu-N) 3232~3477(O-H)

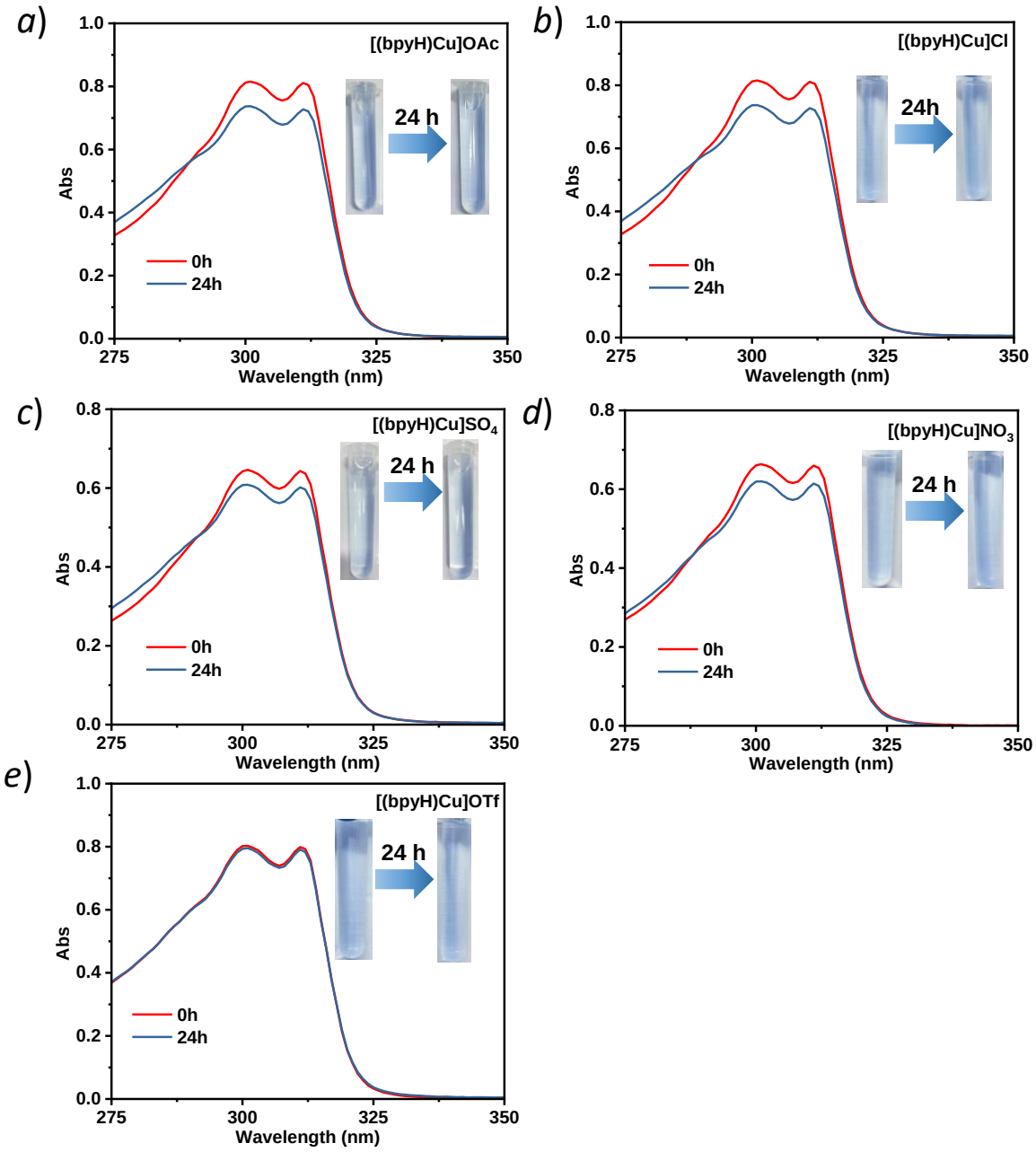

Figure S7. UV-Vis of 0.5 mM [(bpyH)Cu]X dissolution in a 0.1 M pH 12.5 NaOH/NaOAc buffer at 0 hours and 24 hours.

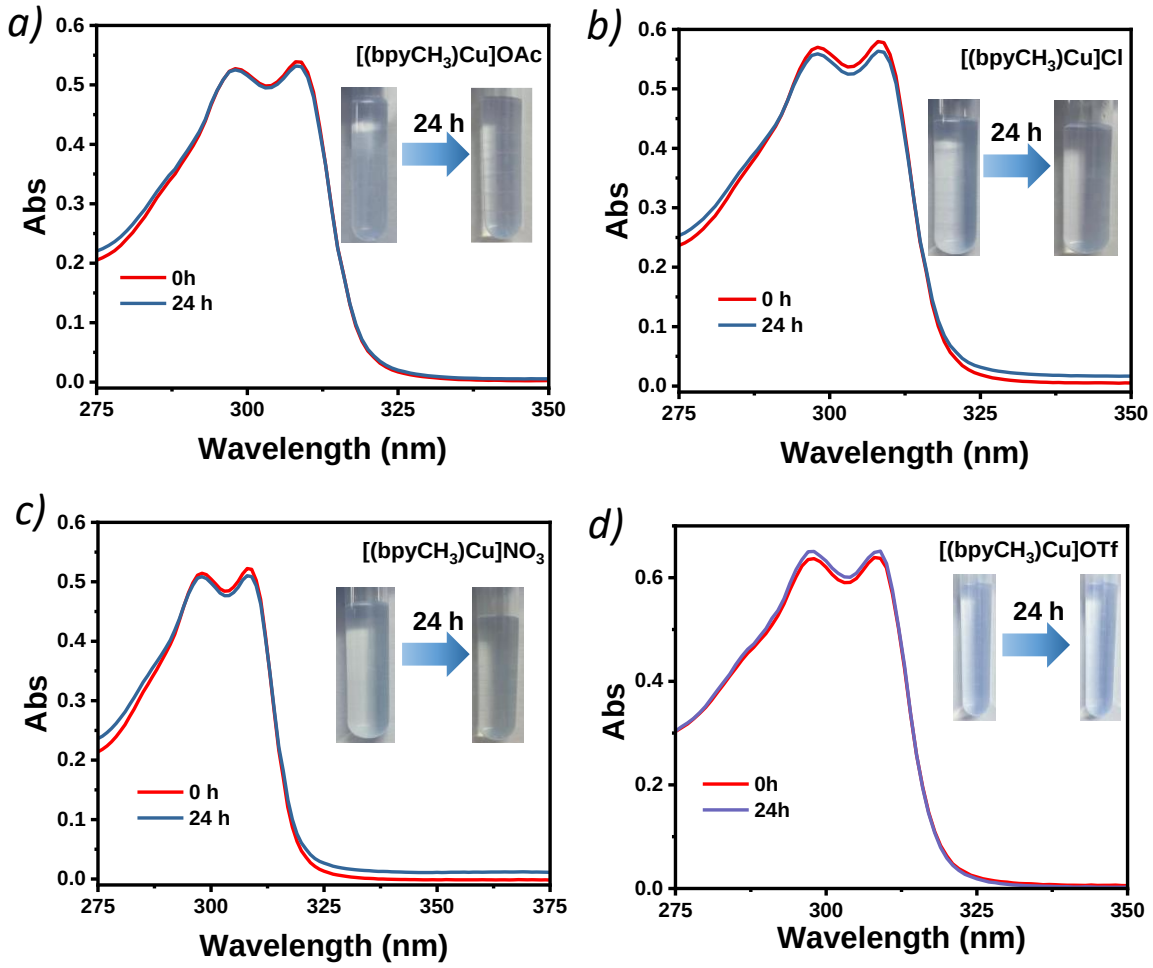

Figure S8. UV-Vis of 0.5 mM [(bpyCH$_3$)Cu]X dissolution in a 0.1 M pH 12.5 NaOH/NaOAc buffer at 0 hours and 24 hours.

The optimized pH conditions.

According to the previous investigation[2-3, 6], there exists monomer/dimer equilibrium, but the major species at pH 12.5 is $(bpy)Cu(OH)_2$.

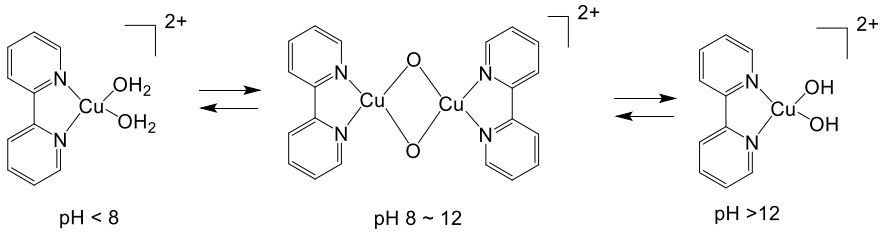

To determine the optimal pH conditions for these complexes, cyclic voltammograms (CV) were measured in pH 11.8 to 13. The irreversible pH-dependent oxidative waves in CV correspond to the catalytic water oxidation. The peak current and peak water oxidation potential versus pH are shown in **Figure S9-S17**. Although the higher the pH, the higher the peak current is, the peak potential was also increased to an uneconomical value. Hence, pH 12.5 was confirmed as the optimal buffer condition.

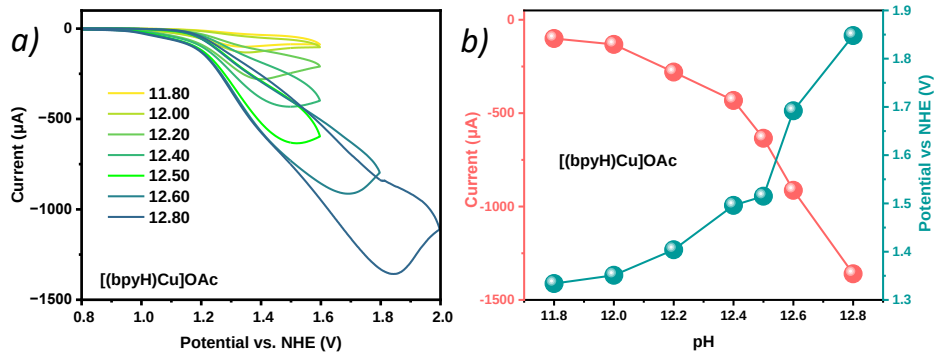

Figure S9. a) CVs of aqueous solutions containing 1 mM of [(bpyH)Cu]OAc under various pH 0.1M NaOH/NaOAc buffers. b) The water oxidation current and potential of 1 mM Cu-R in the pH range of 11.8-12.8.

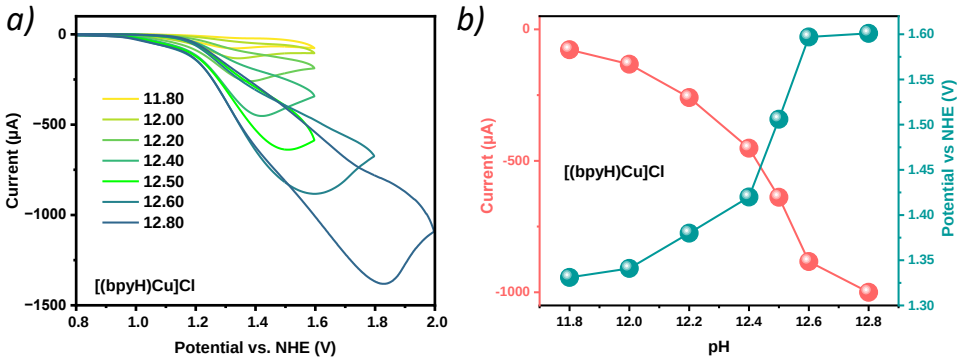

Figure S10. a) CVs of aqueous solutions containing 1 mM of [(bpyH)Cu] under various pH 0.1M NaOH/NaOAc buffers. b) The water oxidation current and potential of 1 mM Cu-R in the pH range of 11.8-12.8.

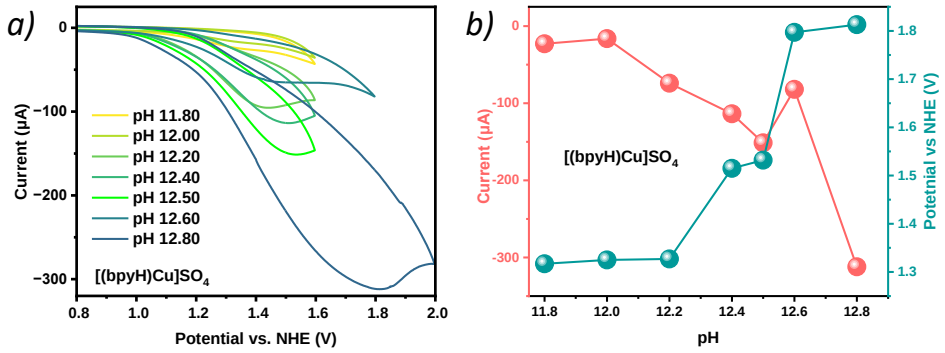

Figure S11. a) CVs of aqueous solutions containing 1 mM of $[(bpyH)Cu]SO_4$ under various pH 0.1M NaOH/NaOAc buffers. b) The water oxidation current and potential of 1 mM Cu-R in the pH range of 11.8-12.8.

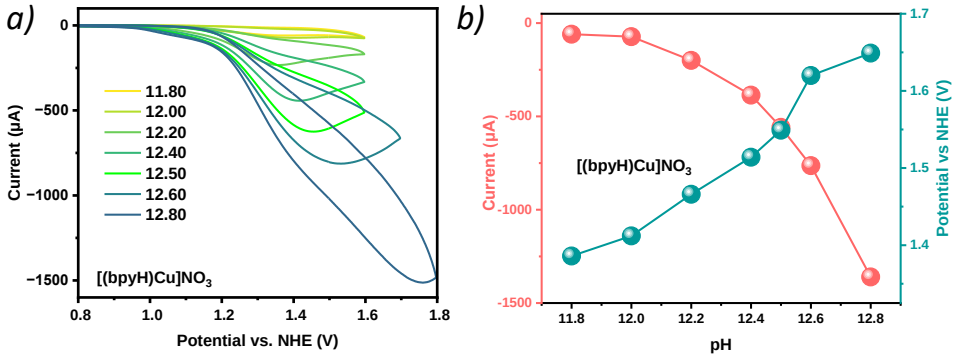

Figure S12. a) CVs of aqueous solutions containing 1 mM of $[(bpyH)Cu]NO_3$ under various pH 0.1M NaOH/NaOAc buffers. b) The water oxidation current and potential of 1 mM Cu-R in the pH range of 11.8-12.8.

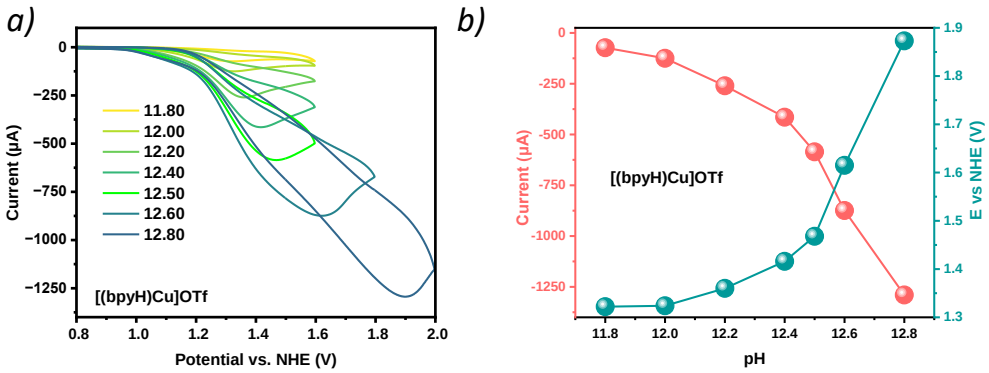

Figure S13. a) CVs of aqueous solutions containing 1 mM of [(bpyH)Cu]OTf under various pH 0.1M NaOH/NaOAc buffers. b) The water oxidation current and potential of 1 mM Cu-R in the pH range of 11.8-12.8.

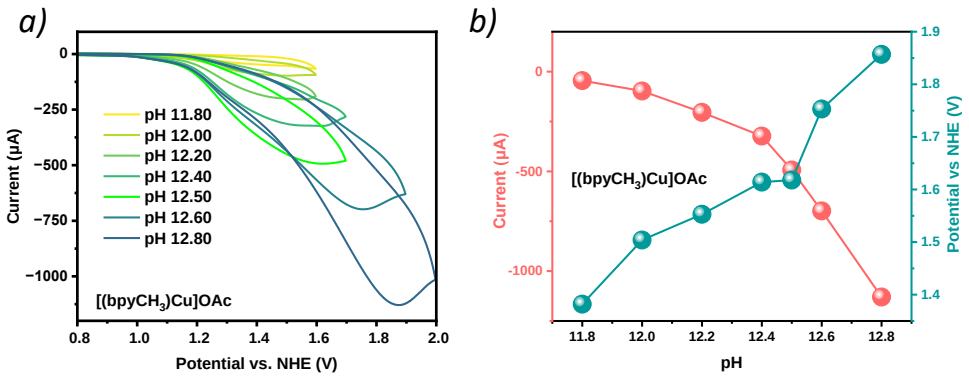

Figure S14. a) CVs of aqueous solutions containing 1 mM of [(bpyCH$_3$)Cu]OAc under various pH 0.1M NaOH/NaOAc buffers. b) The water oxidation current and potential of 1 mM Cu-R in the pH range of 11.8-12.8.

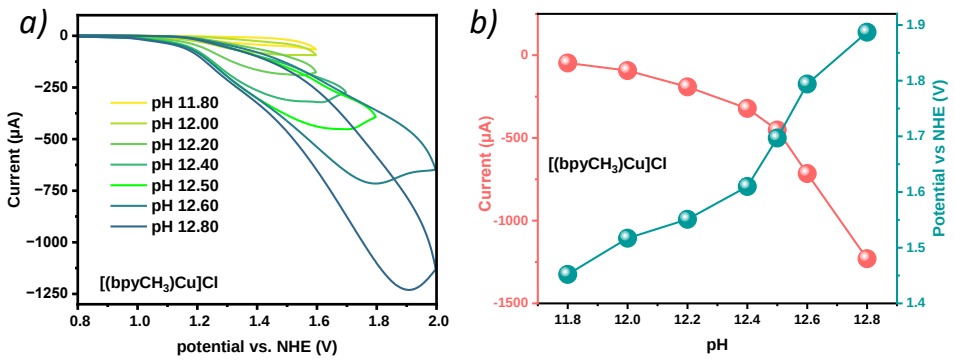

Figure S15. a) CVs of aqueous solutions containing 1 mM of [(bpyCH$_3$)Cu]Cl under various pH 0.1 M NaOH/NaOAc buffers. b) The water oxidation current and potential of 1 mM Cu-R in the pH range of 11.8-12.8.

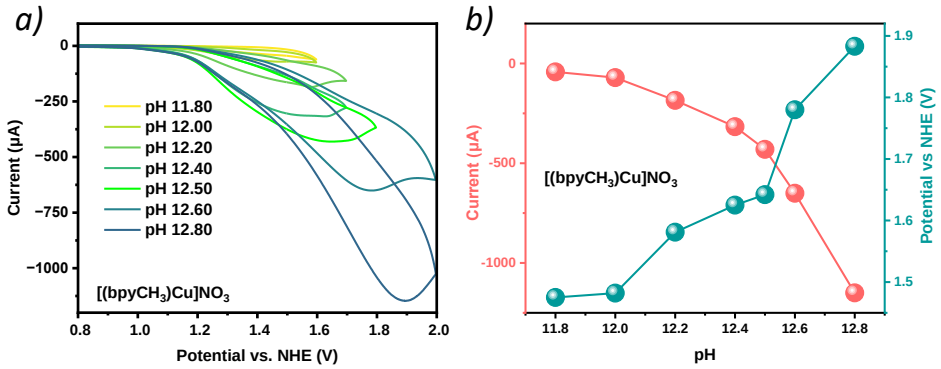

Figure S16. a) CVs of aqueous solutions containing 1 mM of [(bpyCH$_3$)Cu]NO$_3$ under various pH 0.1 M NaOH/NaOAc buffers. b) The water oxidation current and potential of 1 mM Cu-R in the pH range of 11.8-12.8.

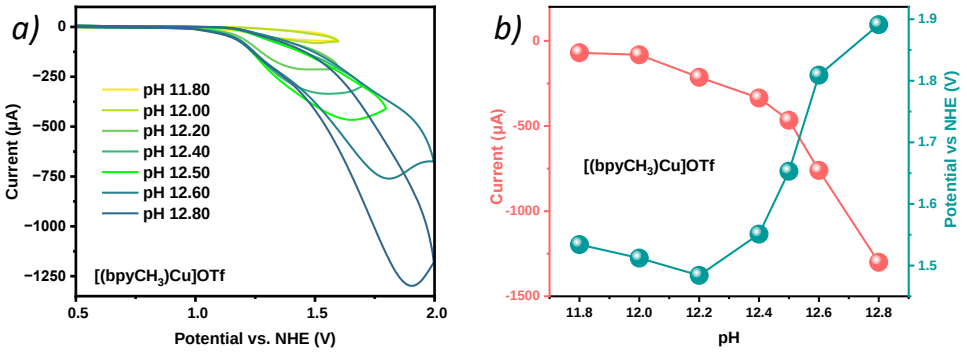

Figure S17. a) CVs of aqueous solutions containing 1 mM of [(bpyCH$_3$)Cu]OTf under various pH 0.1 M NaOH/NaOAc buffers. b) The water oxidation current and potential of 1 mM Cu-R in the pH range of 11.8-12.8.

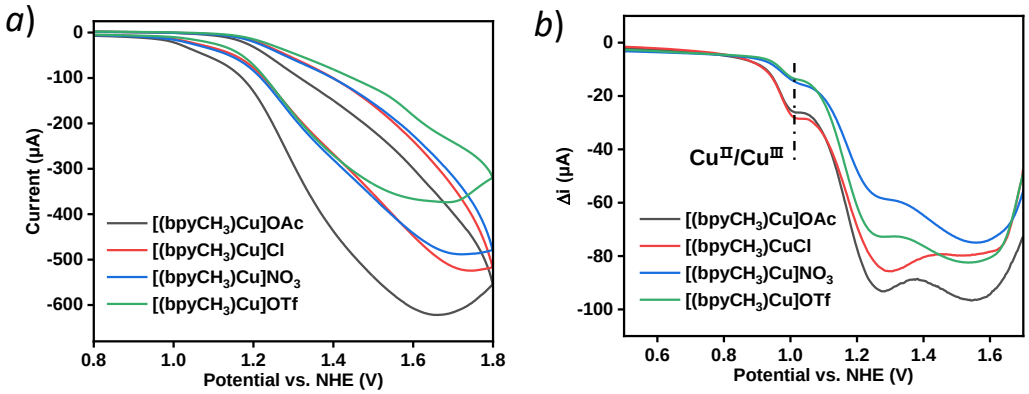

Figure S18. a) CVs, b) SWVs of aqueous solutions containing 1 mM of [(bpyCH$_3$)Cu]X under 0.1 M pH 12.5 NaOH/NaOAc buffers.

Coordination ability index, a^{TM}

$$a^{TM} = \log (c+s)/u$$

where c, s and u are the number of structures with the group coordinated, semi coordinated and uncoordinated, respectively. A positive value of a^{TM} indicates that the group has more chance to coordinate to a transition metal atom than to remain uncoordinated in its presence. The larger the positive value of a^{TM}, the greater its coordinating ability.

Catalytic performances evaluation

The TOF can be estimated according to equation S1-S3 based on previous studies[1, 7].

$$i_d = 0.4633nFAc_{cat}\sqrt{\frac{nFvD}{RT}} \quad (S1)$$

$$i_{cat} = n_{cat}FAc_{cat}\sqrt{k_{cat}D} \quad (S2)$$

$$\frac{i_{cat}}{i_d} = 1.424\sqrt{\frac{k_{cat}}{v}} \quad (S3)$$

In these equations, n is the number of electrons transferred in the uncatalyzed reaction ($Cu^{II/I}$ reduction, n=1), F is the Faraday's constant (F = 96485 C/mol), A is the area of the working electrode (A = 0.07 cm^2), c_{cat} is the bulk concentration of the catalyst, D is the diffusion coefficient, R is the gas constant, T is the absolute temperature, n_{cat} is the number of electrons transferred during the process in which the catalytic reaction occurs, hence n_{cat} is 4, and k_{cat} is the apparent first-order rate constant[8-9], which is often used to evaluate the water oxidation performance for molecular catalysts[10]. By plotting i_{cat}/i_d versus $V^{-1/2}$, we can evaluate the k_{cat} by the slope. To keep the consistency, we choose the last four points to do the calculations. Though these evaluation

methods may not be accurate to reflect their real TOFs but can be used to compare their relative values.

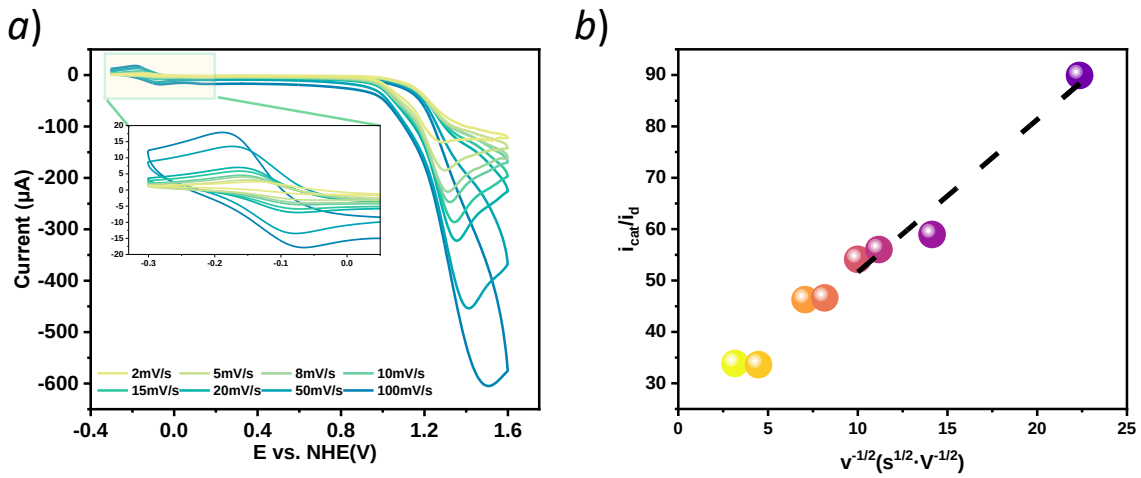

Figure S19. (a) CVs of [(bpyH)Cu]OAc solution under various scan rates (pH 12.5, 0.1 M NaOH/NaOAc); (b) corresponding linear fitting plot of i_{cat}/i_d vs $v^{-1/2}$ for TOF calculations.

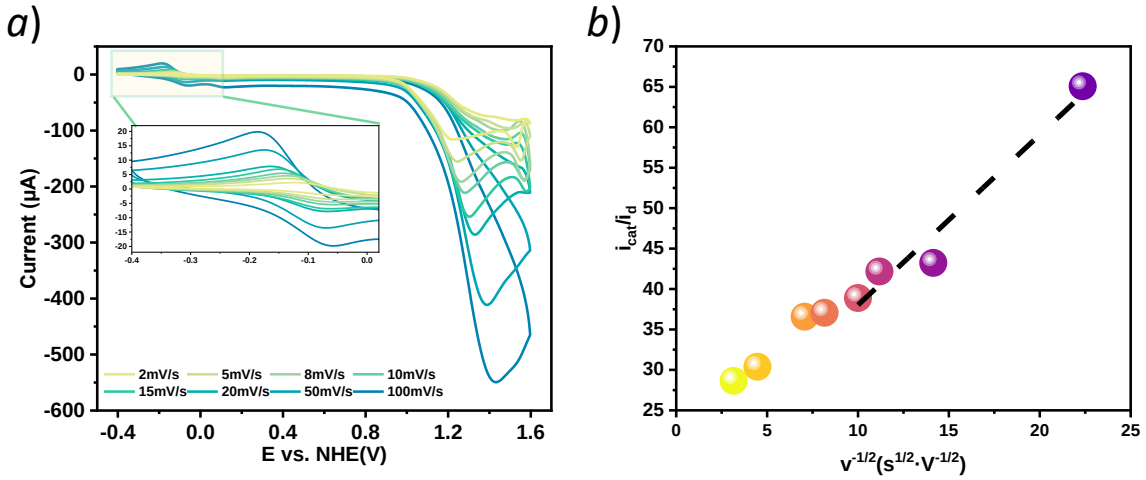

Figure S20. (a) CVs of [(bpyH)Cu]Cl solution under various scan rates (pH 12.5, 0.1 M NaOH/NaOAc); (b) corresponding linear fitting plot of i_{cat}/i_d vs $v^{-1/2}$ for TOF calculations.

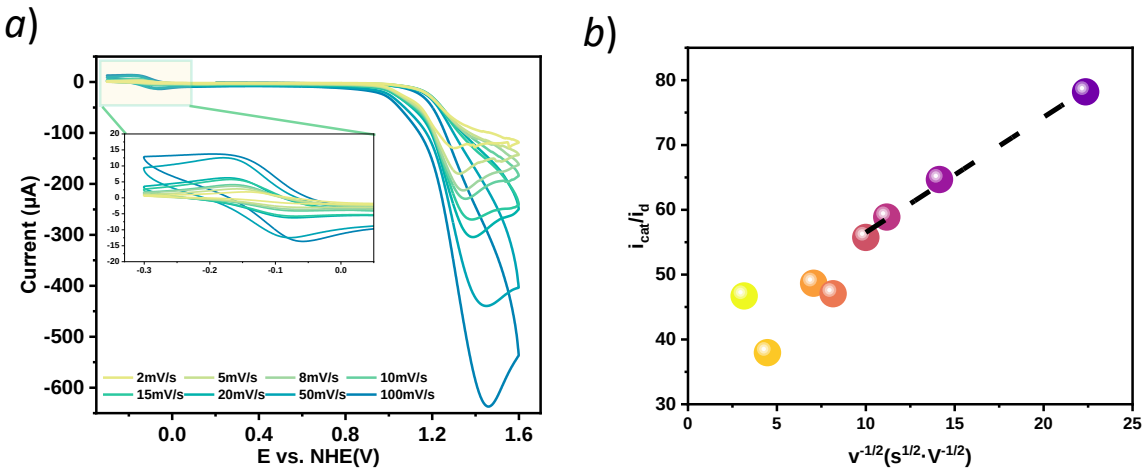

Figure S21. (a) CVs of [(bpyH)Cu]SO_4 solution under various scan rates (pH 12.5, 0.1 M NaOH/NaOAc); (b) corresponding linear fitting plot of i_{cat}/i_d vs $v^{-1/2}$ for TOF calculations.

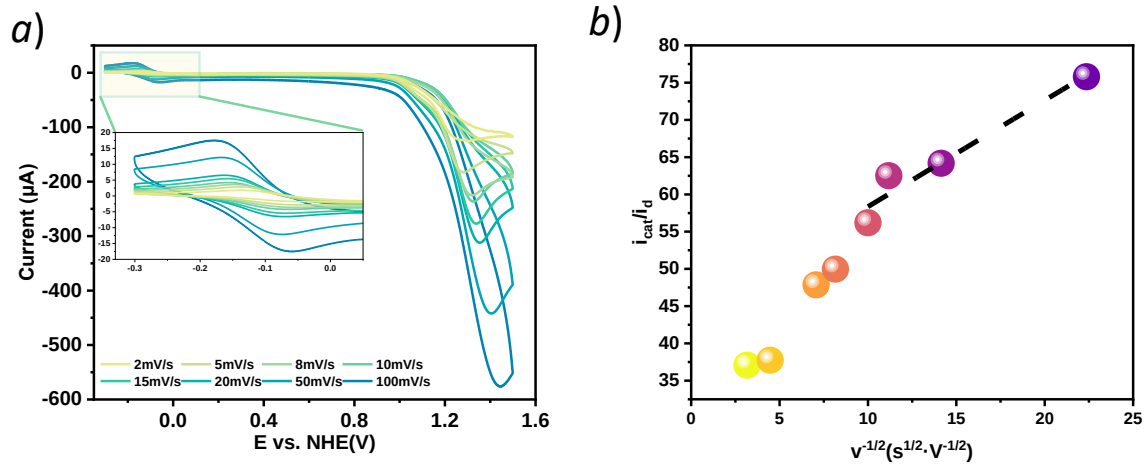

Figure S22. (a) CVs of [(bpyH)Cu]NO_3 solution under various scan rates (pH 12.5, 0.1 M NaOH/NaOAc); (b) corresponding linear fitting plot of i_{cat}/i_d vs $v^{-1/2}$ for TOF calculations.

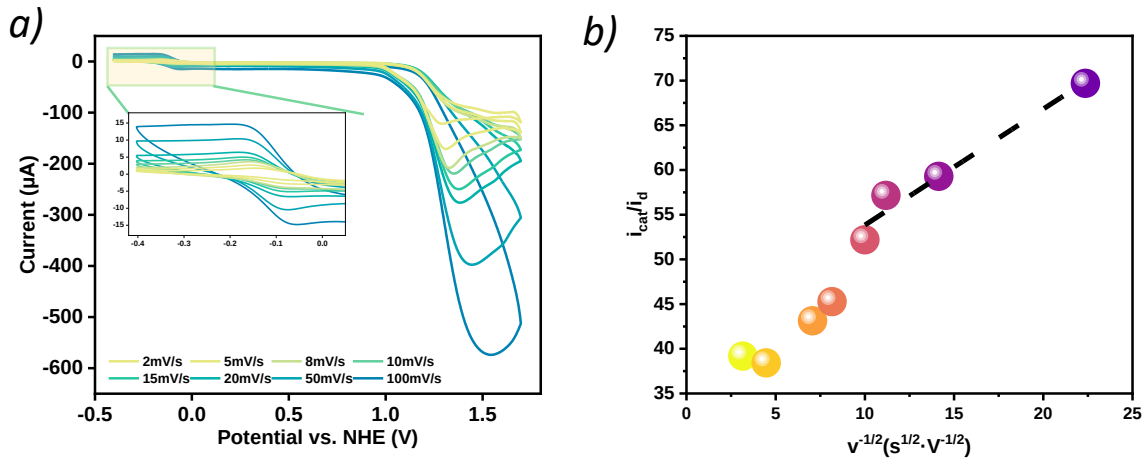

Figure S23. (a) CVs of [(bpyH)Cu]OTf solution under various scan rates (pH 12.5, 0.1 M NaOH/NaOAc); (b) corresponding linear fitting plot of i_{cat}/i_d vs $v^{-1/2}$ for TOF calculations.

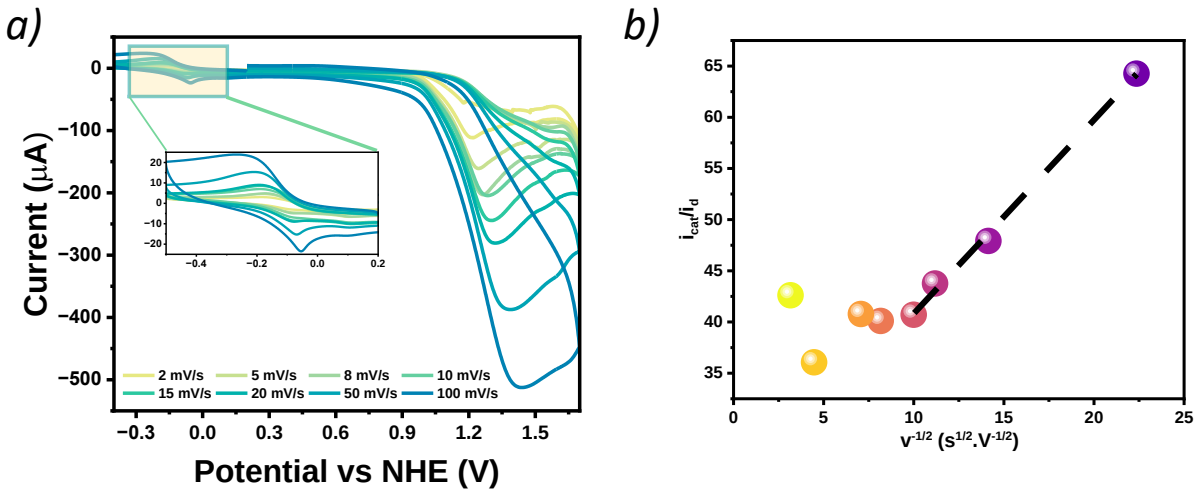

Figure S24. (a) CVs of [(bpyCH$_3$)Cu]OAc solution under various scan rates (pH 12.5, 0.1 M NaOH/NaOAc); (b) corresponding linear fitting plot of i_{cat}/i_d vs $v^{-1/2}$ for TOF calculations.

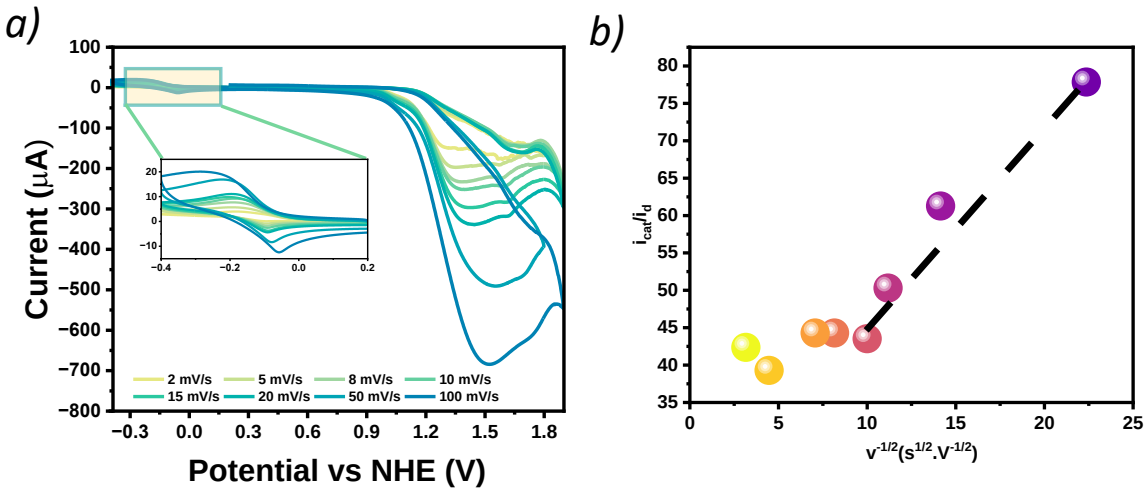

Figure S25. (a) CVs of [(bpyCH$_3$)Cu]Cl solution under various scan rates (pH 12.5, 0.1 M NaOH/NaOAc); (b) corresponding linear fitting plot of i_{cat}/i_d vs $v^{-1/2}$ for TOF calculations.

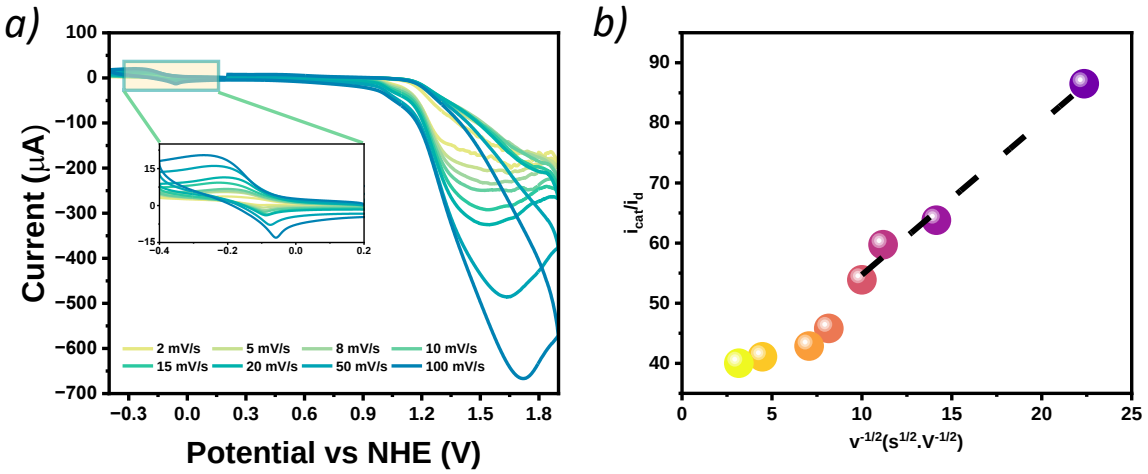

Figure S26. (a) CVs of [(bpyCH$_3$)Cu]NO$_3$ solution under various scan rates (pH 12.5, 0.1 M NaOH/NaOAc); (b) corresponding linear fitting plot of i_{cat}/i_d vs $v^{-1/2}$ for TOF calculations.

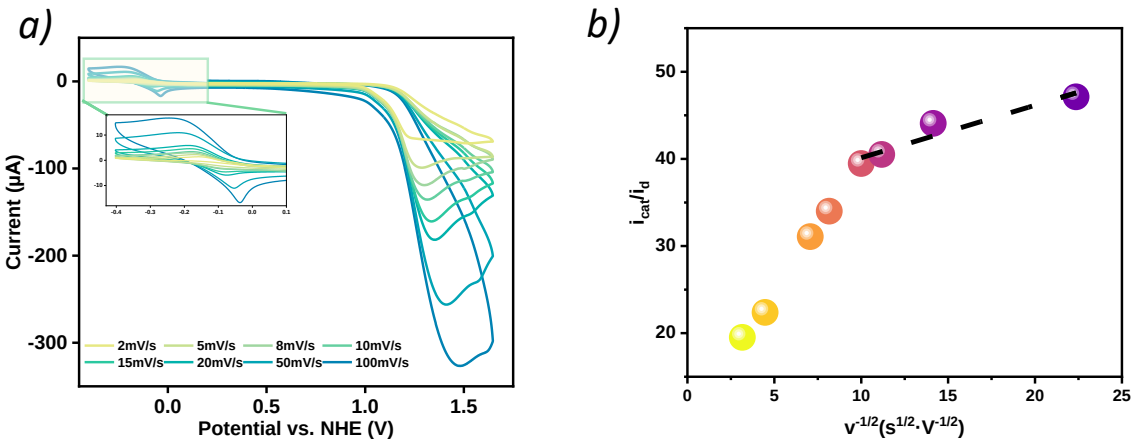

Figure S27. (a) CVs of [(bpyCH$_3$)Cu]OTf solution under various scan rates (pH 12.5, 0.1 M NaOH/NaOAc); (b) corresponding linear fitting plot of i_{cat}/i_d vs $v^{-1/2}$ for TOF calculations.

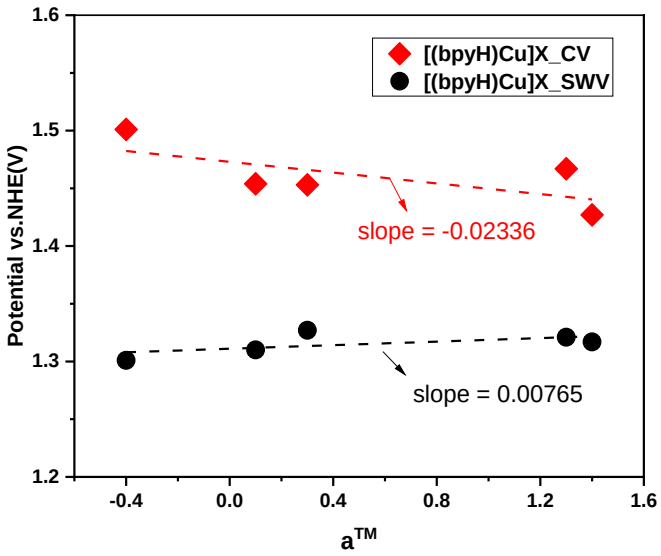

Figure S28. The relationship between a^{TM} and peak potentials of (red) CVs and (Black) SWVs Condition: 1mM [(bpyH)Cu]X in 0.1 M pH 12.50 NaOH/NaOAc buffers.

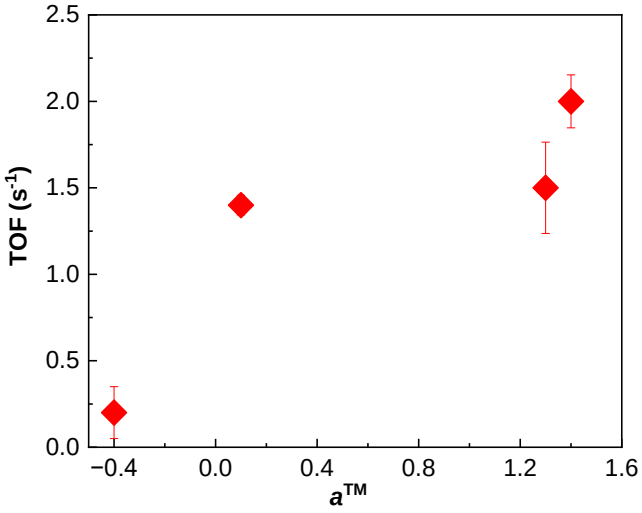

Figure S29. The relationship of TOF versus coordinating ability index a^{TM} for complex [(bpyCH$_3$)Cu]X.

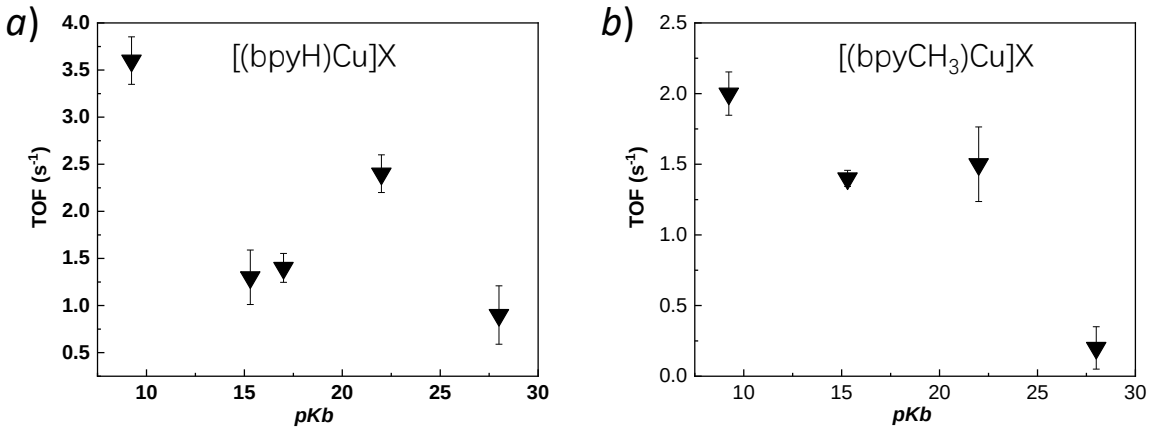

Figure S30. The relationship of TOF versus pKb.

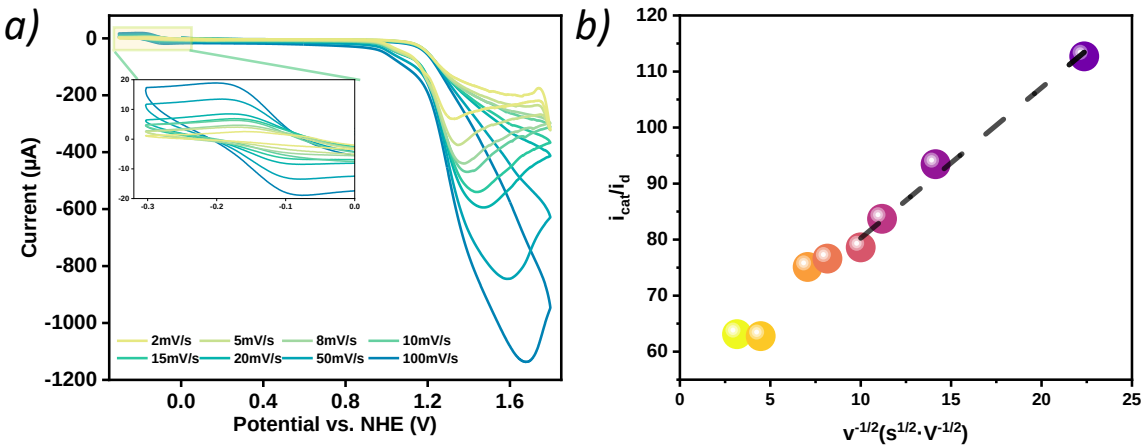

Figure S31. (a) CVs of [(bpyH)Cu]OAc solution under various scan rates (pH 12.5, 0.1 M NaOH/NaCl buffer); (b) corresponding linear fitting plot of i_{cat}/i_d vs $v^{-1/2}$ for TOF calculations.

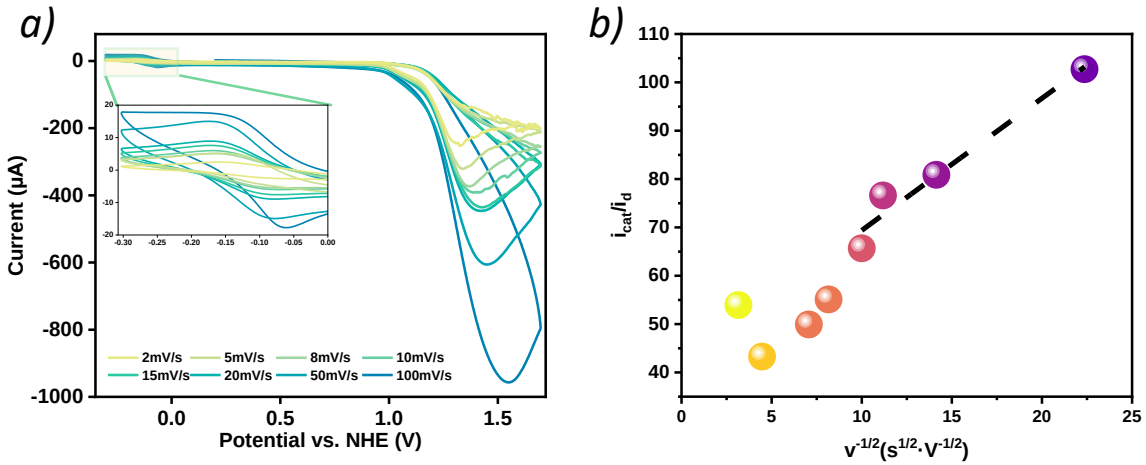

Figure S32. (a) CVs of [(bpyH)Cu]OAc solution under various scan rates (pH 12.5, 0.1 M NaOH/NaOTf buffer); (b) corresponding linear fitting plot of i_{cat}/i_d vs $v^{-1/2}$ for TOF calculations**.**

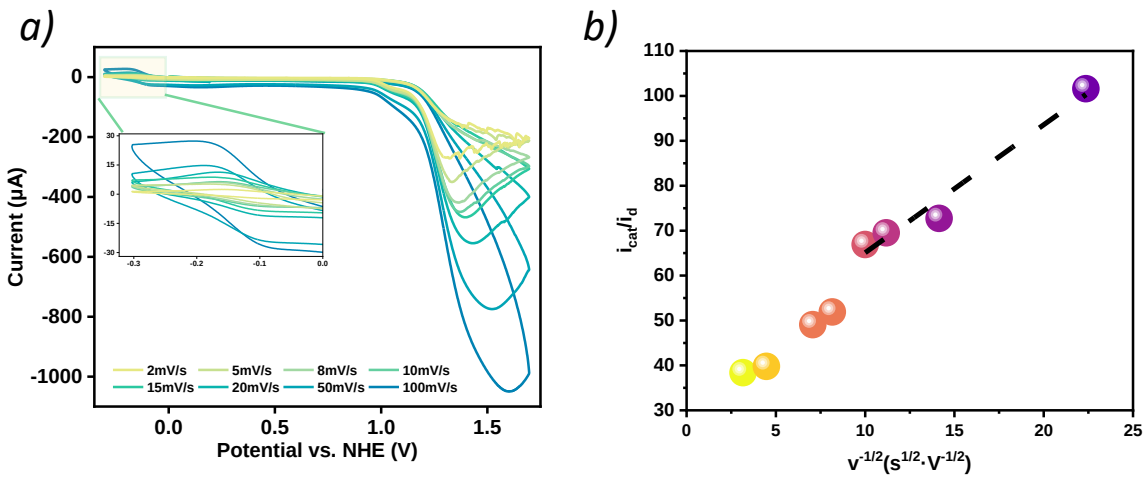

Figure S33. (a) CVs of [(bpyH)Cu]OAc solution under various scan rates (pH 12.5, 0.1 M NaOH/Na_2SO_4 buffer); (b) corresponding linear fitting plot of i_{cat}/i_d vs $v^{-1/2}$ for TOF calculations.

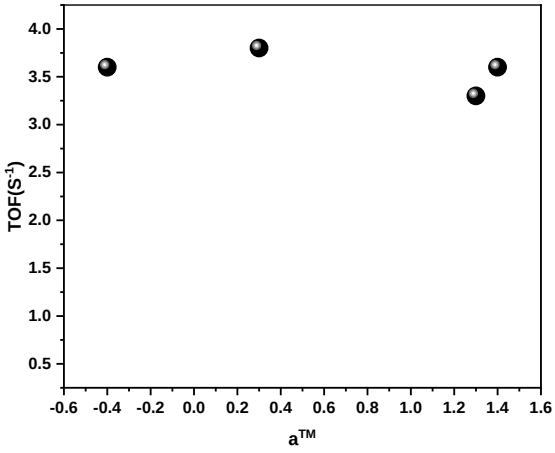

Figure S34. The relationship between a^{TM} of different anionic and TOF of [(bpyH)Cu]OAc in different buffer solutions of pH 12.50 (0.1 M NaOH/NaOAc, 0.1 M NaOH/NaCl, 0.1 M NaOH/Na_2SO_4 and 0.1 M NaOH/NaOTf).

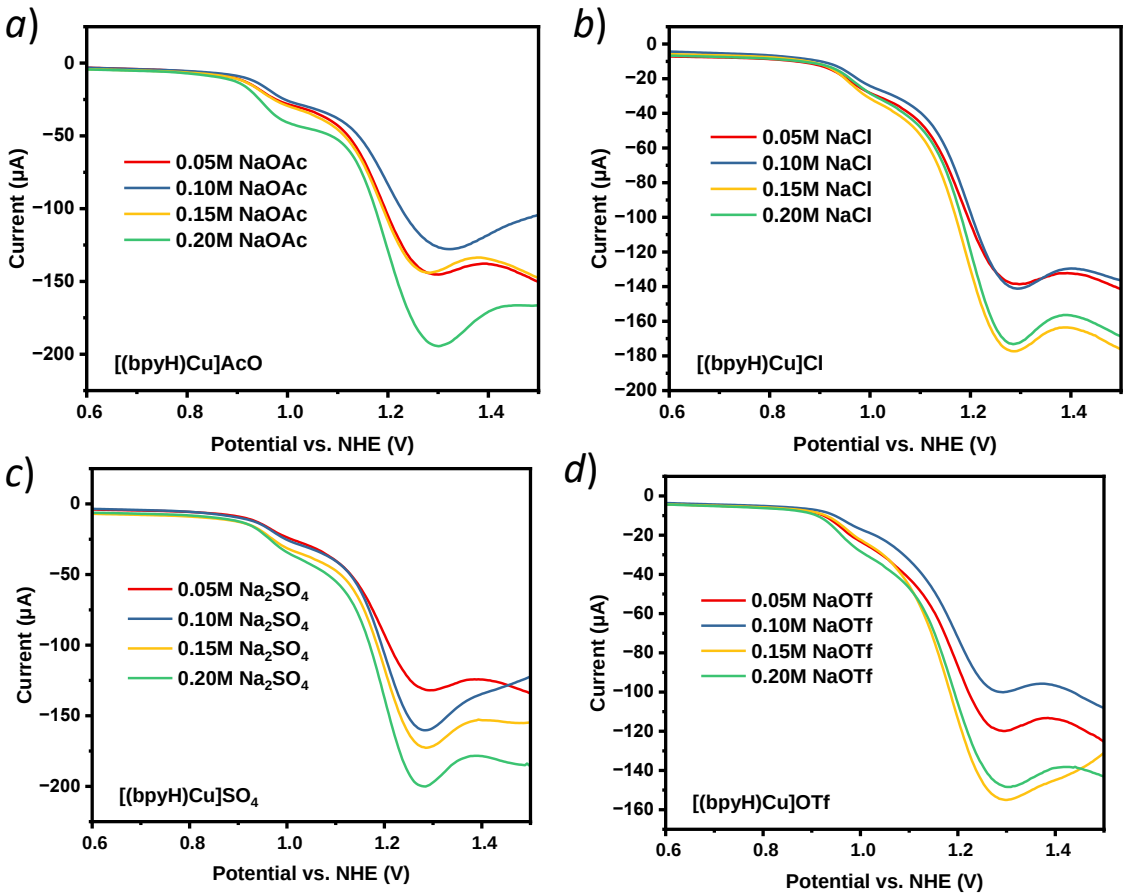

Figure S35. SWVs of aqueous solutions containing 1 mM of [(bpyH)Cu]X under pH 12.5 buffers with various concentrations of anions (0.05 M, 0.1 M, 0.15 M, 0.2 M). Note: The effect of NO_3^- was not measured due to the unavailability of controlled agent $NaNO_3$.

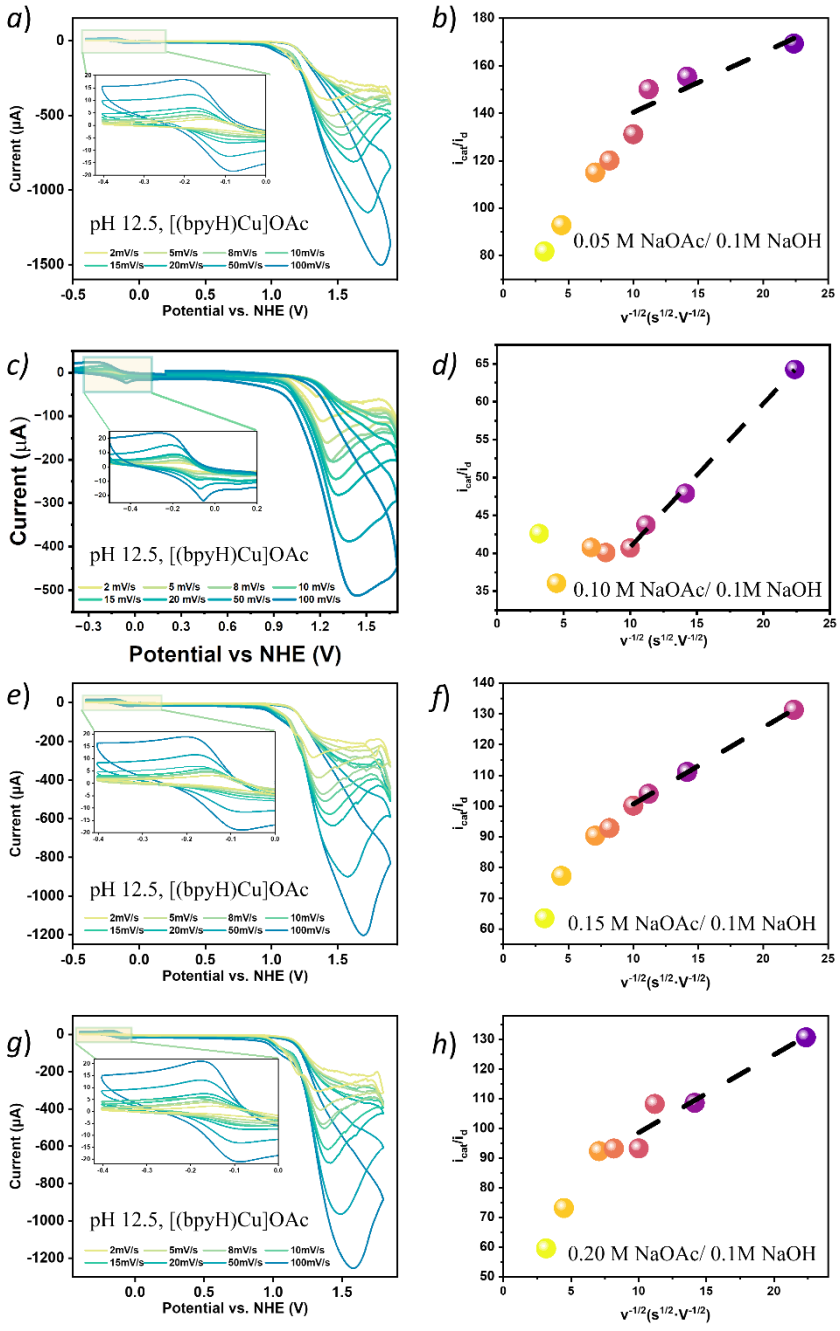

Figure S36. (left) CVs of [(bpyH)Cu]OAc solution under various scan rates (pH 12.5, NaOAc/ 0.1M NaOH, the concentration of NaOAc is labeled on the right column); (right) corresponding linear fitting plot of i_{cat}/i_d vs $v^{-1/2}$ for TOF calculations.

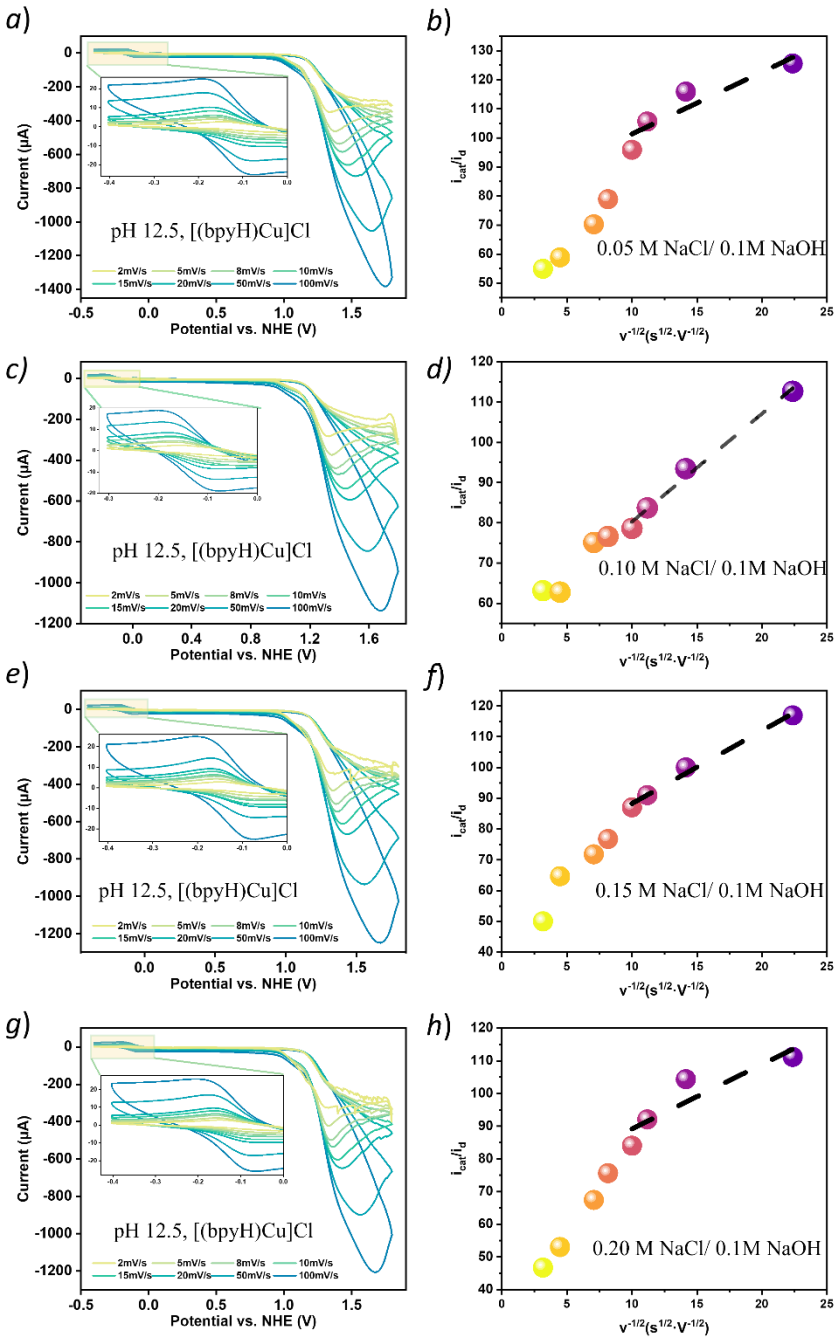

Figure S37. (left) CVs of [(bpyH)Cu]Cl solution under various scan rates (pH 12.5, NaCl/ 0.1M NaOH, the concentration of NaCl is labeled on the right column); (right) corresponding linear fitting plot of i_{cat}/i_d vs $v^{-1/2}$ for TOF calculations.

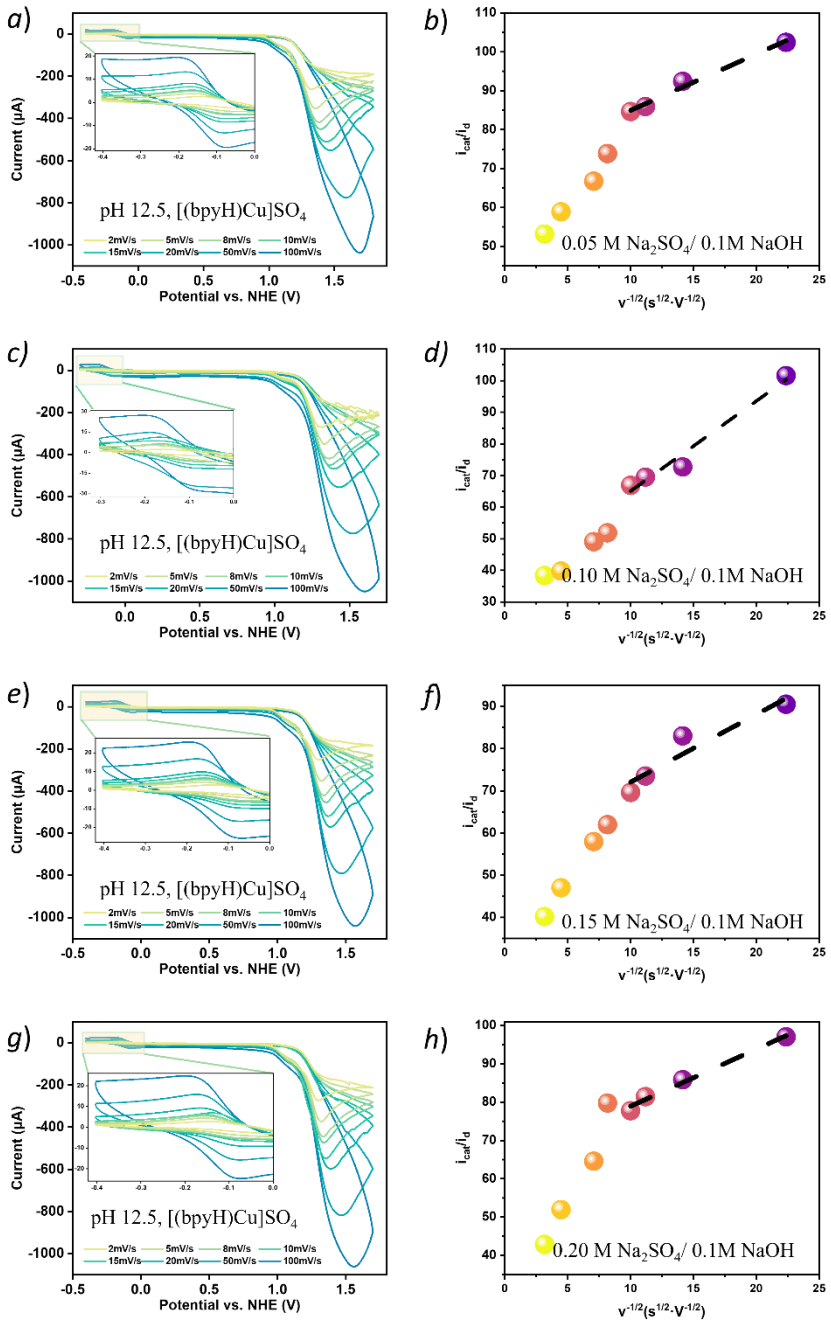

Figure S38. (left) CVs of $[(bpyH)Cu]SO_4$ solution under various scan rates (pH 12.5, Na_2SO_4/ 0.1M NaOH, the concentration of Na_2SO_4 is labeled on the right column); (right) corresponding linear fitting plot of i_{cat}/i_d vs $v^{-1/2}$ for TOF calculations.

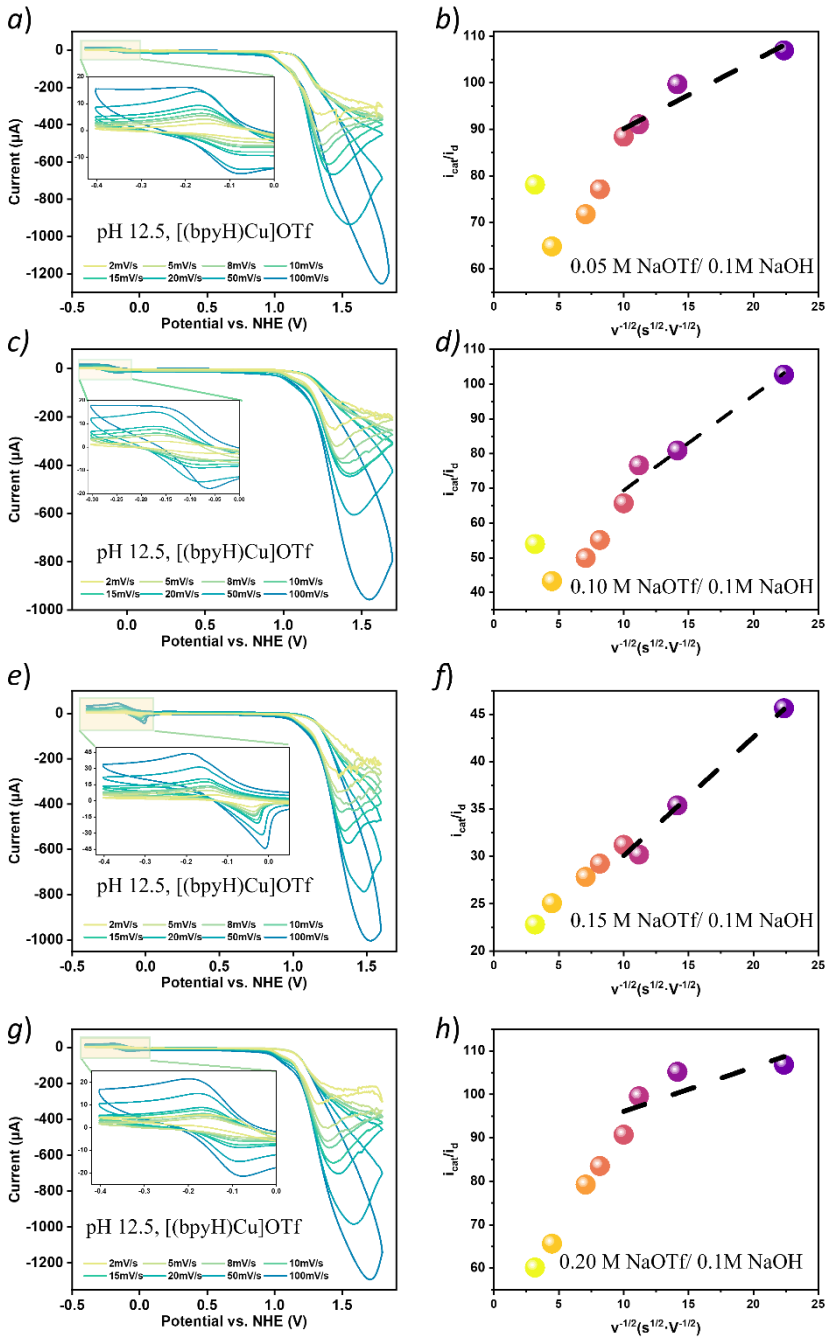

Figure S39. (left) CVs of [(bpyH)Cu]OTf solution under various scan rates (pH 12.5, NaOTf/ 0.1M NaOH, the concentration of NaOTf is labeled on the right column); (right) corresponding linear fitting plot of i_{cat}/i_d vs $v^{-1/2}$ for TOF calculations.

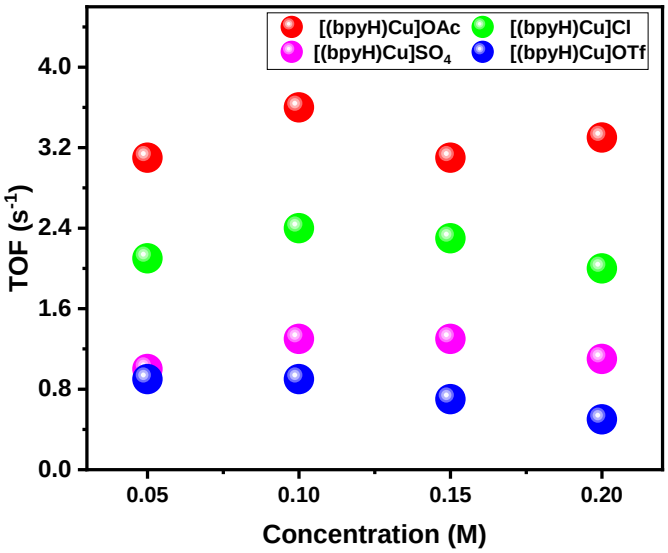

Figure S40. TOF under pH 12.5 buffers with various concentrations of anions (0.05 M, 0.1 M, 0.15 M, 0.2 M). Buffer: a certain concentration of NaX and 0.1 M NaOH.

Spectroelectrochemistry

UV−Vis spectroelectrochemical data for the copper complexes were obtained using the above-mentioned CH Instruments CHI-760E bi-potentiostat coupled to a UV-Visible Agilent Carry60 spectrophotometer and were corrected for the background spectrum of the solvent (i.e. 0.1 M pH NaOH/NaOAc buffers). A standard three-electrode setup was used. The working electrode was a Pt honeycomb microelectrode with a Pt counter electrode and a Ag/AgCl reference electrode. Then the absorption spectrum was recorded at a certain period when holding the applied potentials at 1.15V vs NHE. The generation of Cu(III) was considered completed once the absorption at 308 nm stopped increasing with applied potential.

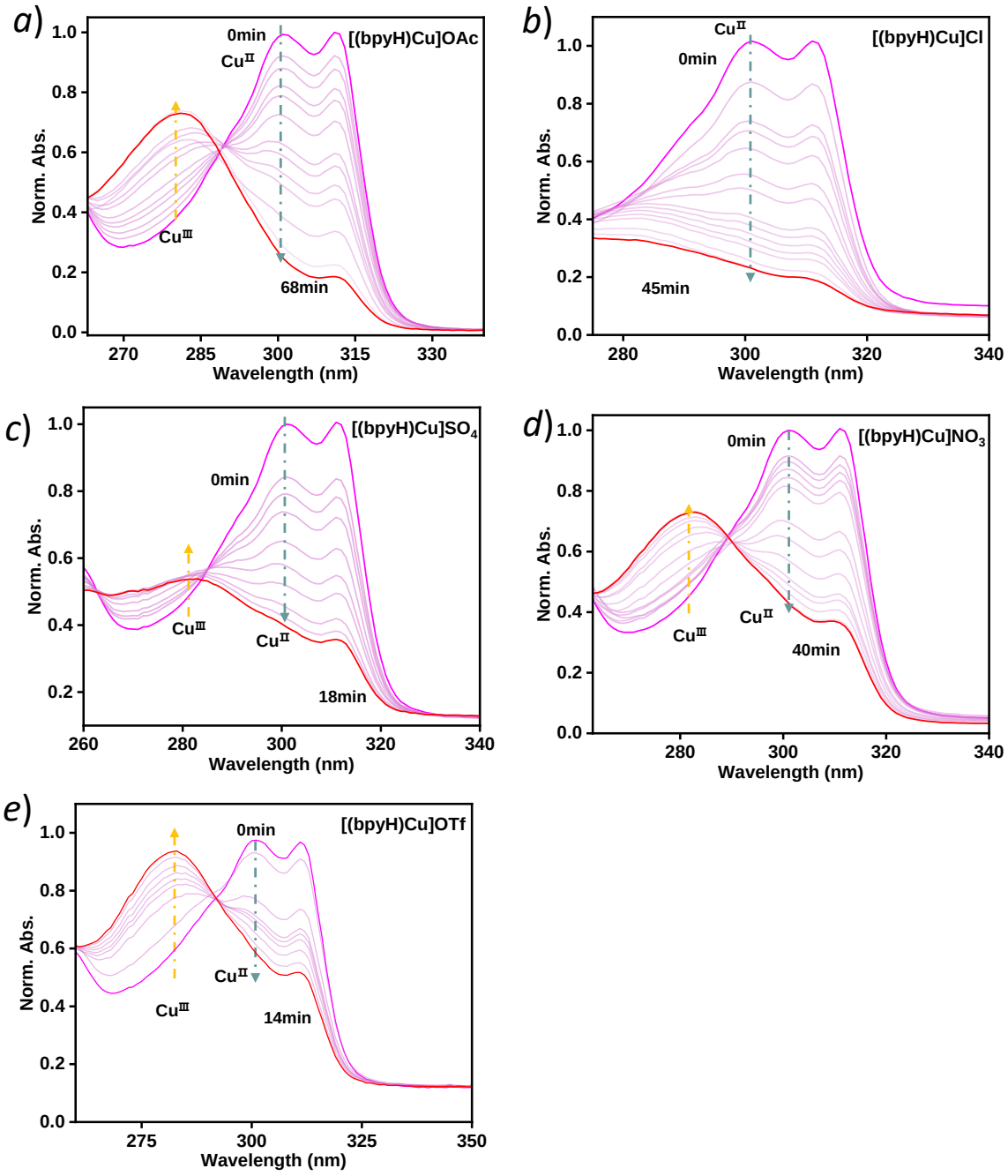

Figure S41. Spectra recorded during the spectroelectrochemical experiment of [(bpyH)Cu]X in 0.1 M pH 12.5 NaOH/NaOAc buffers (applied potential: 1.15 V vs NHE).

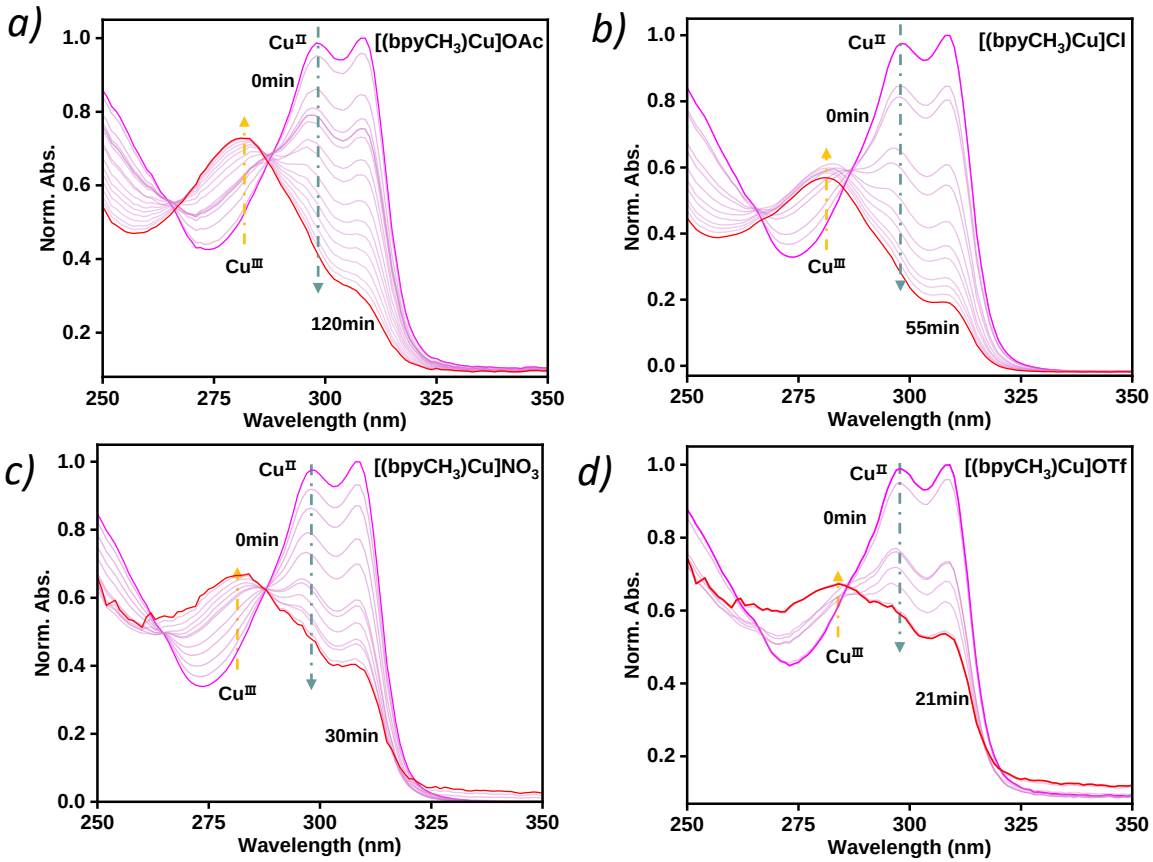

Figure S42. Spectra recorded during the spectroelectrochemical experiment of [(bpyCH$_3$)Cu]X in 0.1 M pH 12.5 NaOH/NaOAc buffers (applied potential: 1.15 V vs NHE).

DFT calculations

The density functional theory (DFT) calculations were carried out by using the density functional theory program DMol^3 in Material Studio (Accelrys, San Diego, CA). The physical wave functions were expanded in terms of numerical basis sets, Dmol^3/GGA-PBE/DNP(3.5) basis set[11] (3), which is comparable to 6-31G** basis sets. The core electrons were treated with DFT semi-core pseudo potentials[12]. The exchange-correlation energy was calculated with Perdew-Burke-Ernzerhof (PBE) generalized gradient approximation (GGA)[13] (2). A Fermi smearing of 0.005 Ha (1 Ha = 627.51 kcal/mol) and a global orbital cutoff of 5.2 Å were employed. The convergence criteria for the geometric optimization and energy calculation were set as follows: (a) a self-consistent field tolerance of 1.0×10^{-6} Ha/atom; (b) an energy tolerance of 1.0×10^{-5} Ha/atom; (c) a maximum force tolerance of 0.002 Ha/Å; (d) a maximum displacement tolerance of 0.005 Å.

Interaction energy calculation

The interaction energy (E_{int}), indicating the intensity of interaction between the components in the system, is derived according to the following equation:

$$E_{int} = E_{total} - \sum E_{each\ component} \quad \text{(S4)}$$

where E_{total} and $E_{each\ component}$ represent the total energy of the system, and the energy of each component, respectively. A negative E_{int} value corresponds to stable adsorption between the components. More negative E_{int} indicates a stronger interaction in the system.

Table S2. The calculated interaction energy of bonding pairs**.**

Complex Forms	Interaction Energy (kcal/mol)
[(bpyH)Cu]OAc	-108.939
[(bpyH)Cu]Cl	-103.571
[(bpyH)Cu]NO_3	-93.167
[(bpyH)Cu]SO_4	-84.061
[(bpyH)Cu]OTf	-77.439
[(bpyCH_3)Cu]OAc	-104.890
[(bpyCH_3)Cu]Cl	-99.648
[(bpyCH_3)Cu]NO_3	-89.252
[(bpyCH_3)Cu]OTf	-74.170

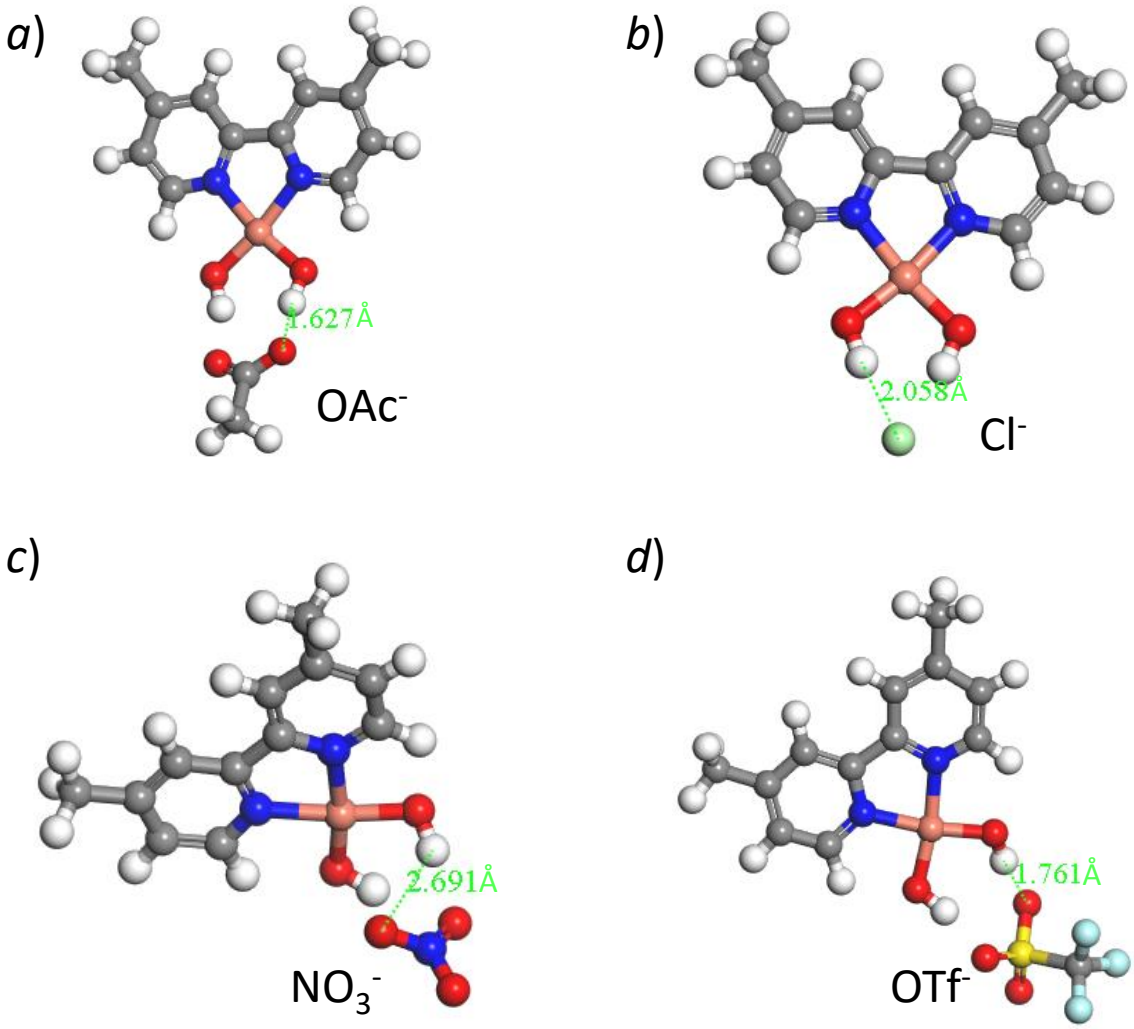

Figure S43. DFT-optimized structures of (a) [($bpyCH_3$)Cu^{III}-OH]OAc, (b) [($bpyCH_3$)Cu^{III}-OH]Cl, (c) [($bpyCH_3$)Cu^{III}-OH]NO_3, (d) [($bpyCH_3$)Cu^{III}-OH]OTf.

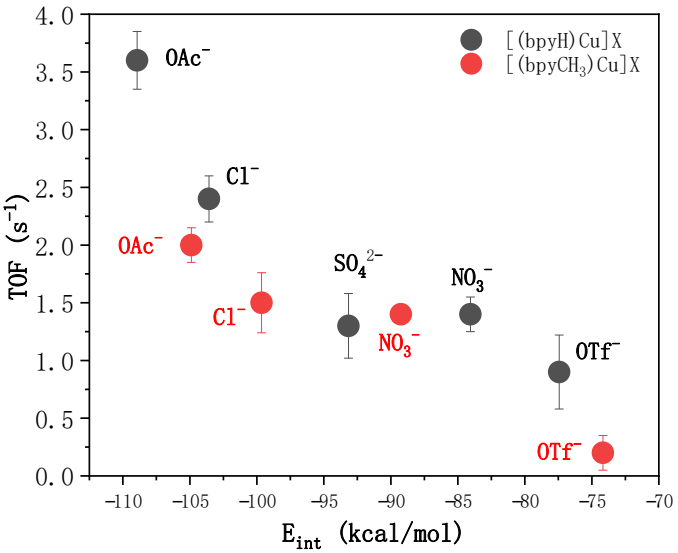

Figure S44. The relationship between TOF and E_{int}.

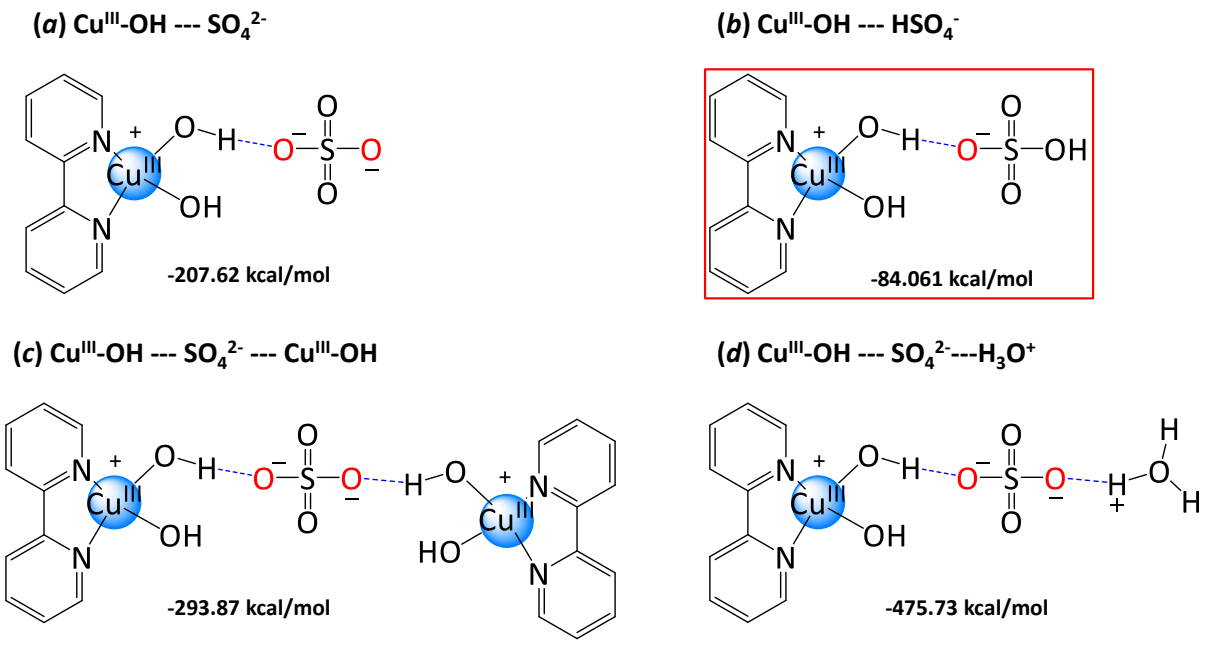

Figure S45. Possible configurations when SO_4^{2-} as the counteranion.

Controlled potential electrolysis (CPE) experiments on glassy carbon working electrode

The electrochemical reduction of O_2 on a glassy carbon electrode was employed to quantify the generated O_2 preliminarily (**Figures S46-S49**). We observed the oxygen reduction current of OAc^- complexes is 160 μA for [(bpyH)Cu]OAc and 100 μA for [(bpyCH$_3$)Cu]OAc), which is higher than OTf^- complexes (66 μA for [(bpyH)Cu]OTf and 42 μA for [(bpyCH$_3$)Cu]OTf). CV and UV-vis spectra analyses were performed before and after electrolysis, as shown in **Figures S51-S54**, demonstrating that the complexes were stable during CPE experiments. Furthermore, to investigate potential Cu-based film deposition on the electrode, an analysis of the glassy carbon surface post-CPE was undertaken (**Figures S55-S56**). The insignificance of water oxidation signals observed after one hour of electrolysis indicates minimal deposition of copper complexes on the electrode surface.

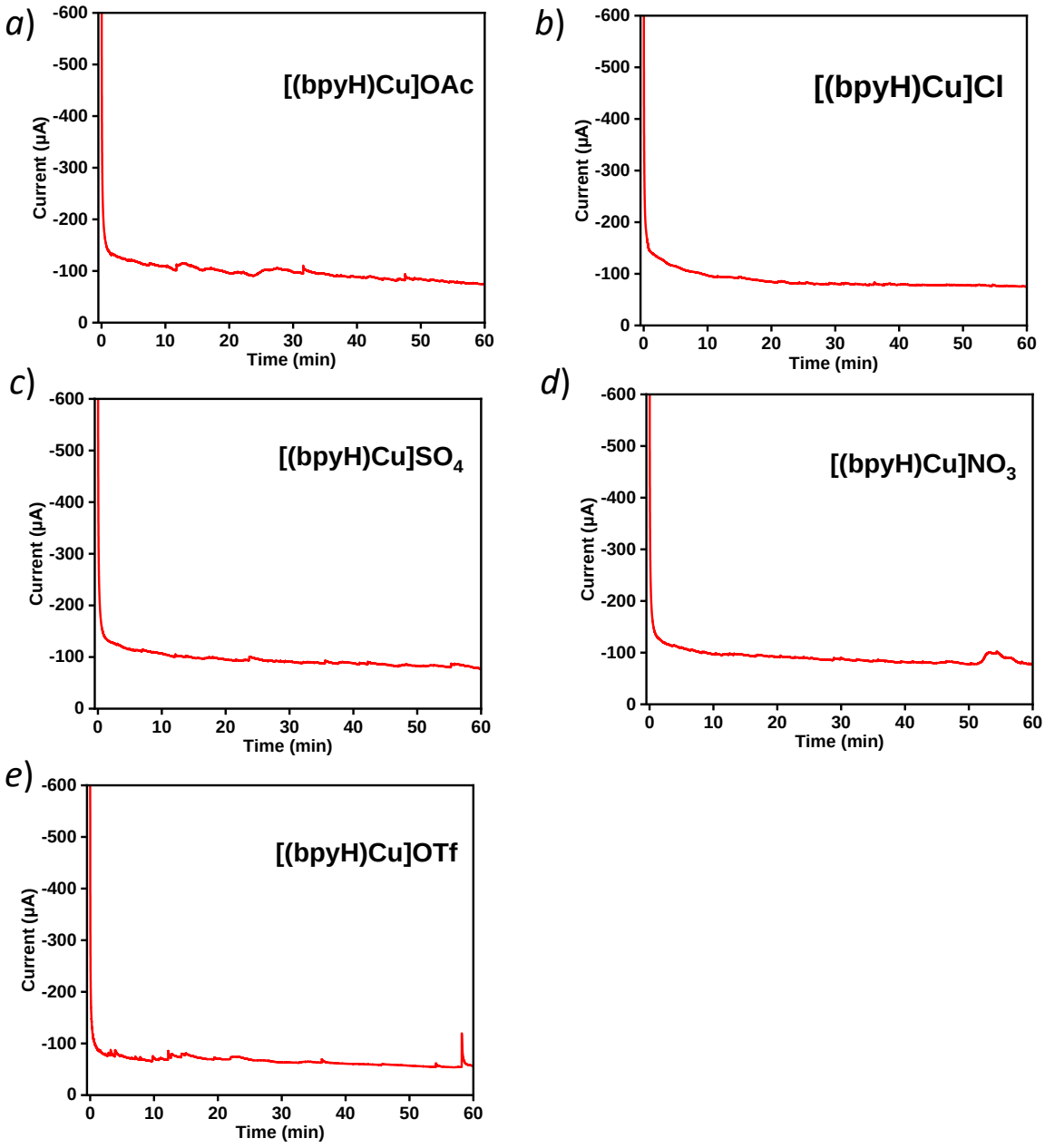

Figure S46. Current of a representative CPE experiment for 1 hour at the potential of 1.6 V vs NHE for [(bpyH)Cu]X.

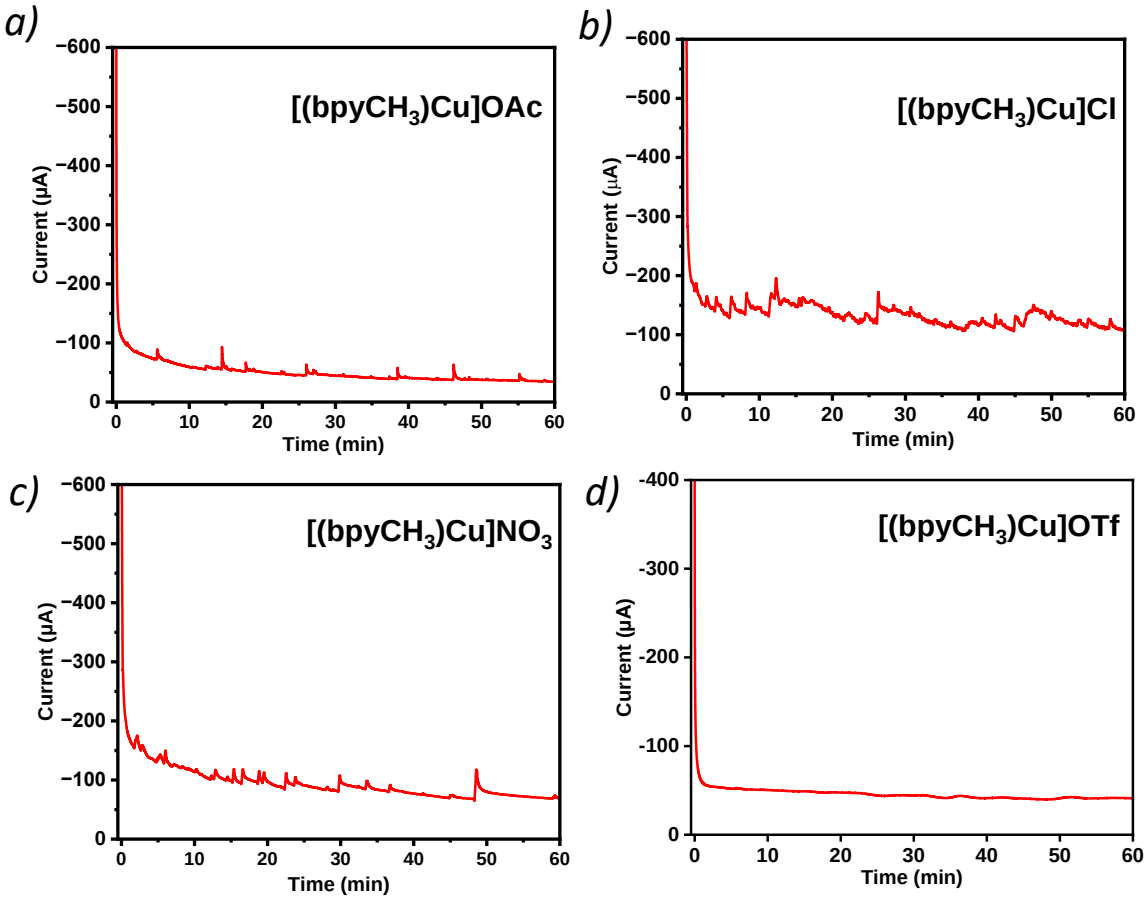

Figure S47. Current of a representative CPE experiment for 1 hour at the potential of 1.6 V vs NHE for [(bpyCH$_3$)Cu]X.

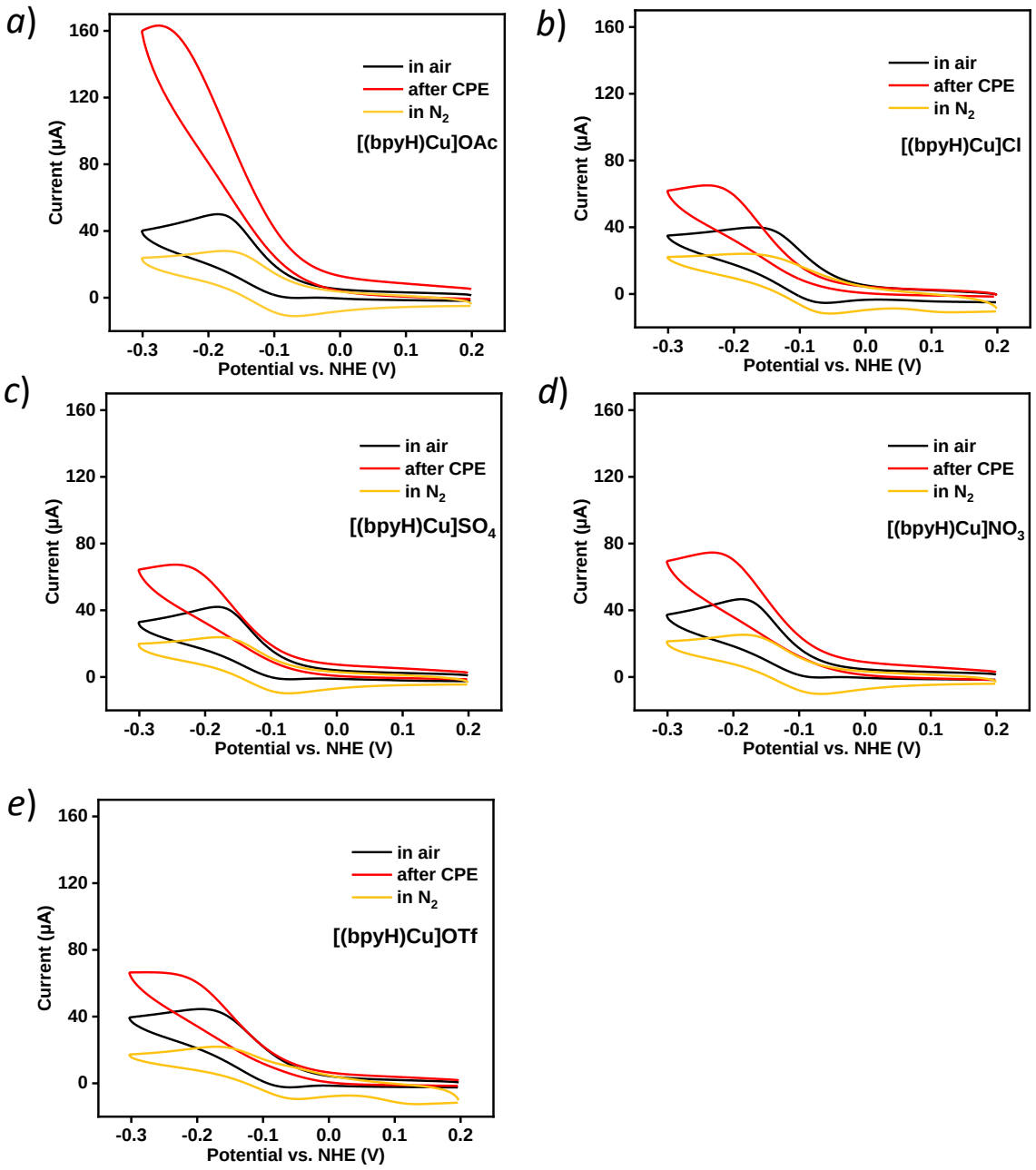

Figure S48. CVs of [(bpyH)Cu]X in N_2, air, and after 1 hour CPE experiment. Conditions: 1 mM [(bpyH)Cu]X in 0.1 M NaOH/NaOAc solution at pH = 12.5.

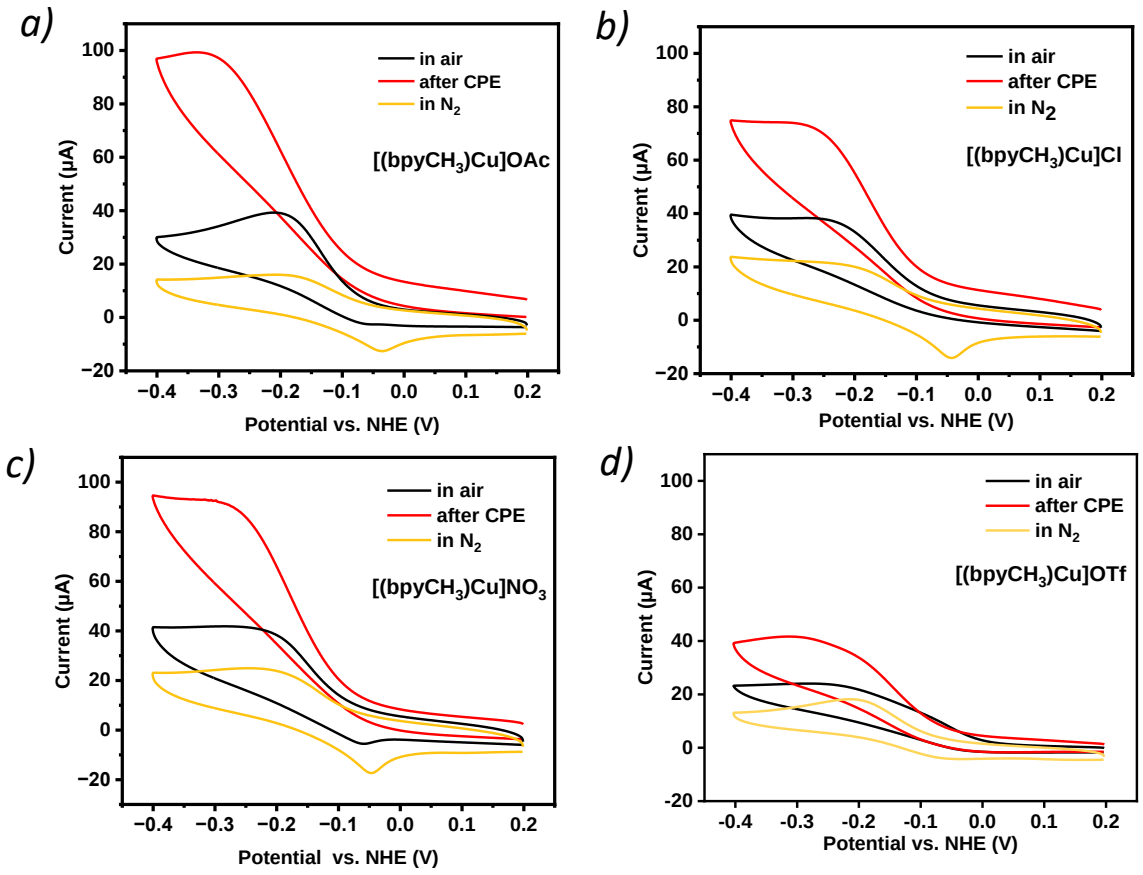

Figure S49. CV of [(bpyCH$_3$)Cu]X in N_2, air, and after 1 hour CPE experiment. Conditions: 1 mM [(bpyCH$_3$)Cu]X in 0.1 M NaOH/NaOAc solution at pH = 12.5.

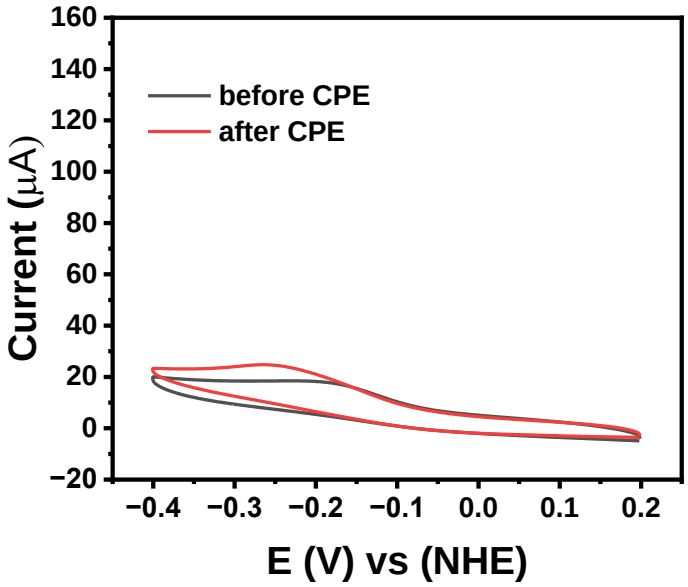

Figure S50. CV of 0.1 M NaOH/NaOAc (pH = 12.5) buffer solution before and after the CPE experiment.

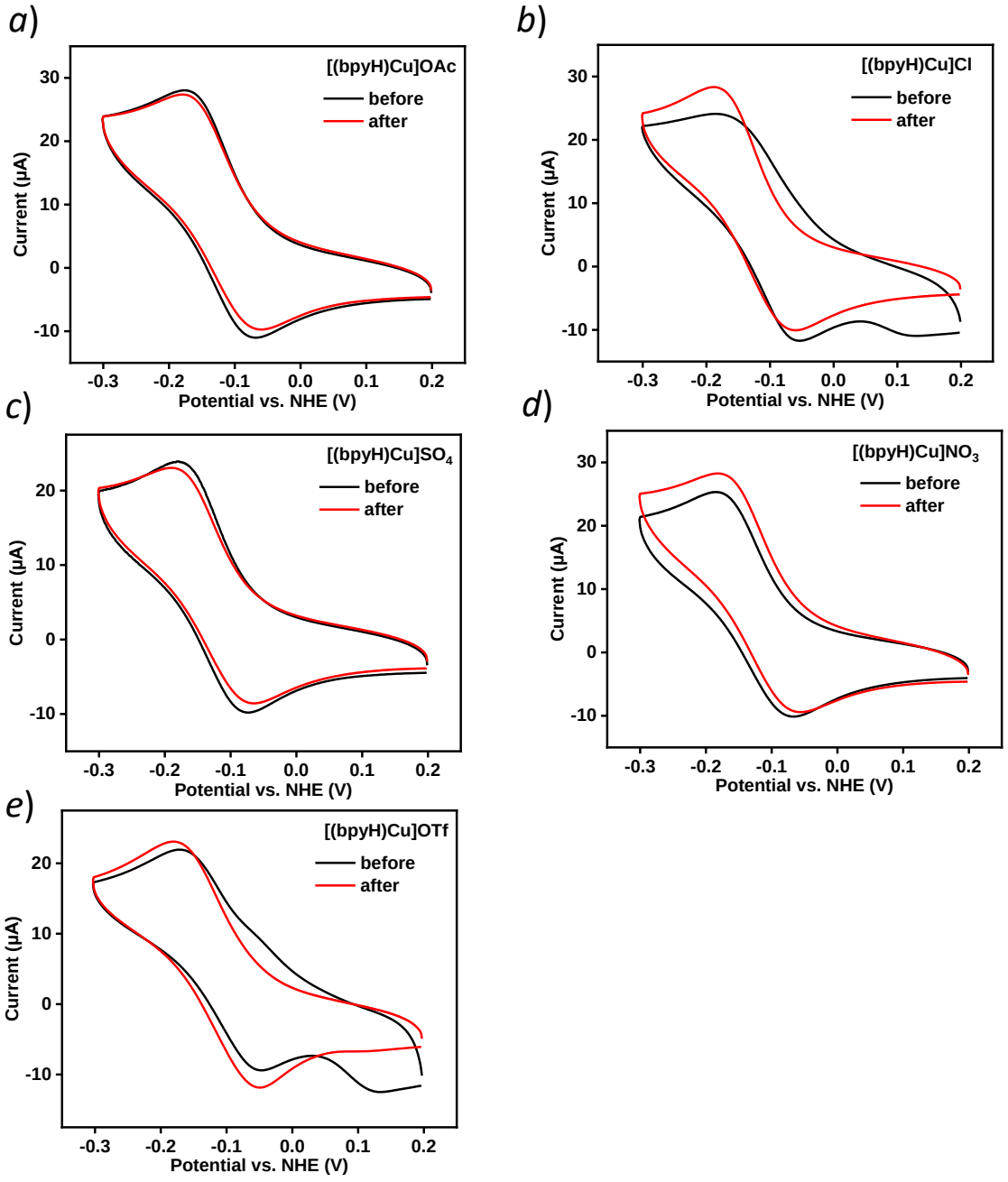

Figure S51. CV of 1 mM [(bpyH)Cu]X showing $Cu^{II/I}$ peaks before and after the CPE experiment.

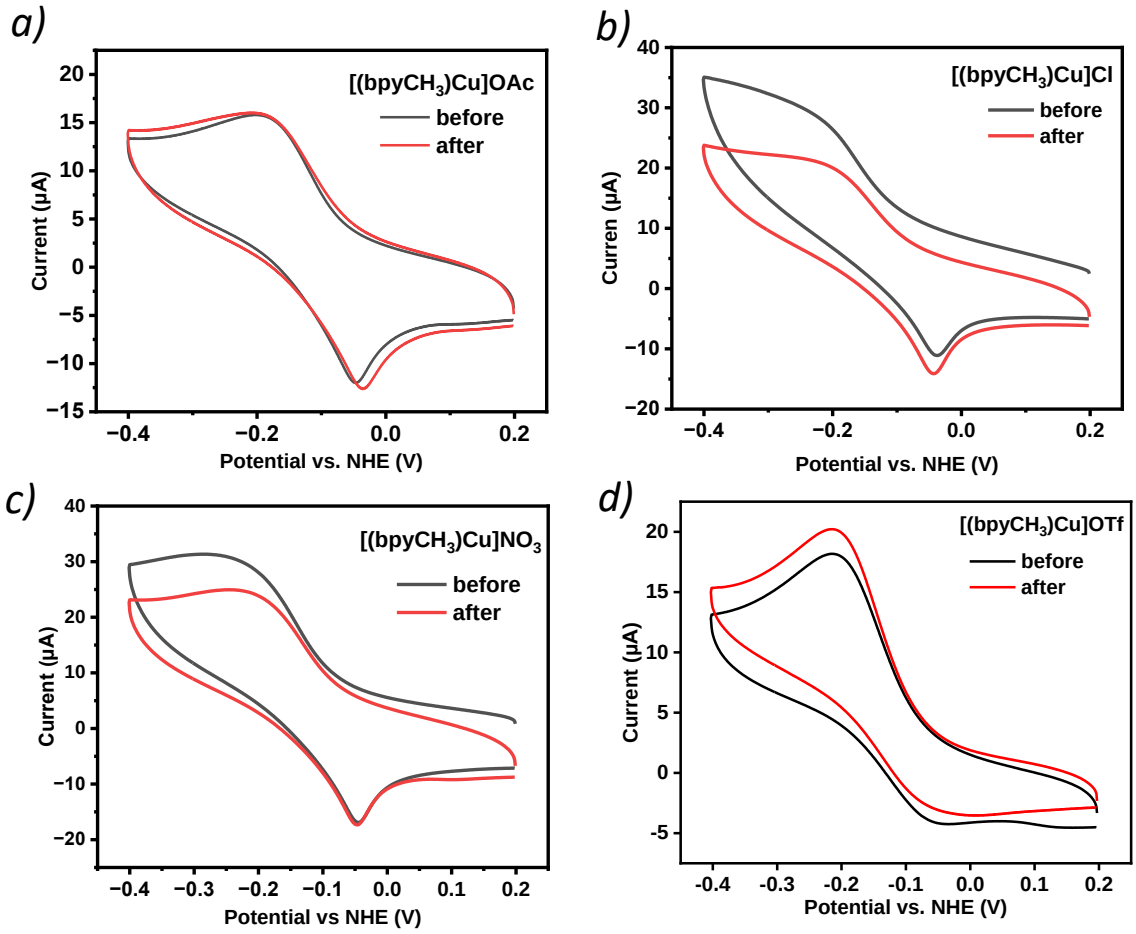

Figure S52. CV of 1 mM [(bpyCH$_3$)Cu]X showing $Cu^{II/I}$ peaks before and after the CPE experiment.

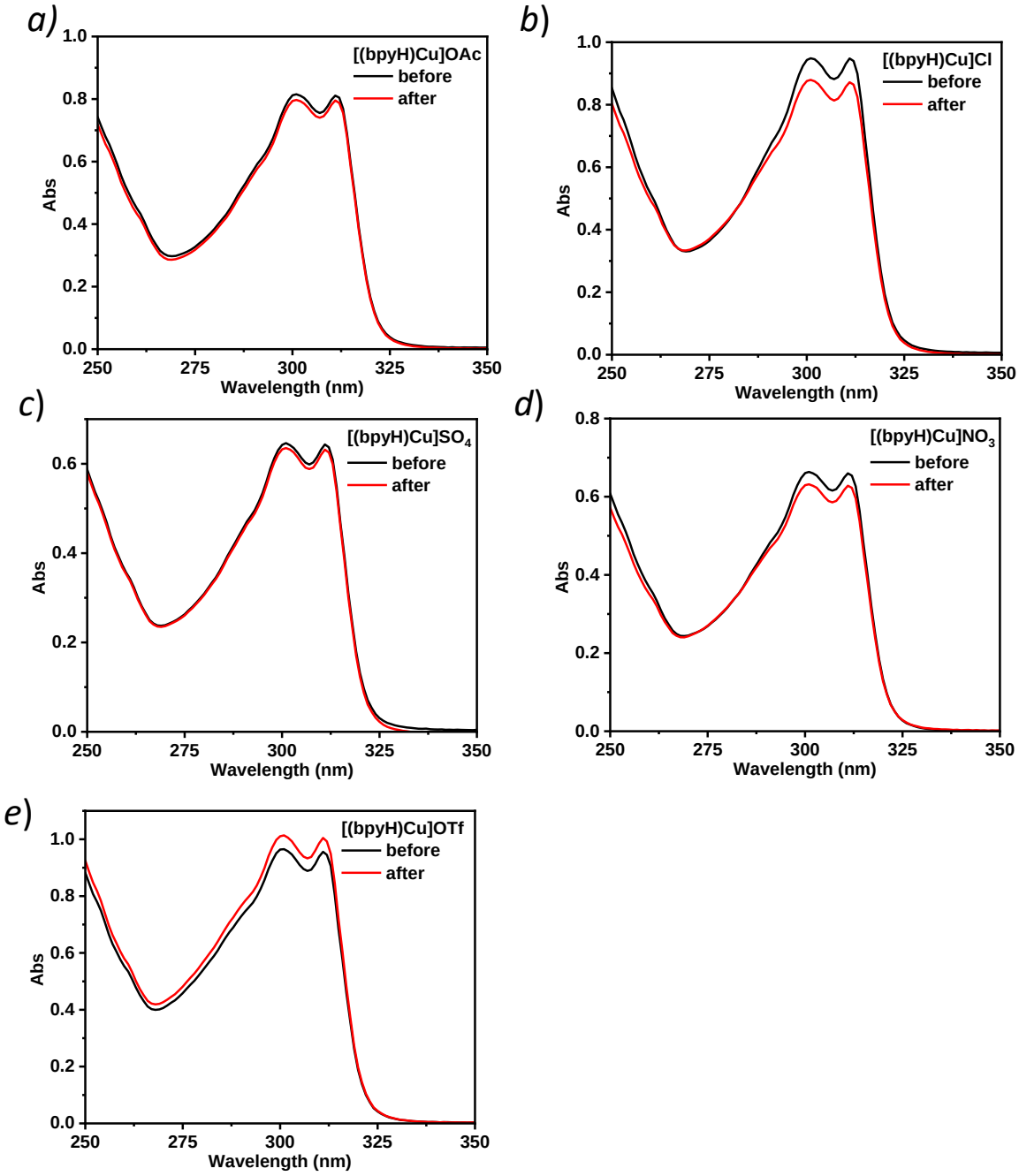

Figure S53. UV-Vis of [(bpyH)Cu]X before and after the CPE experiment.

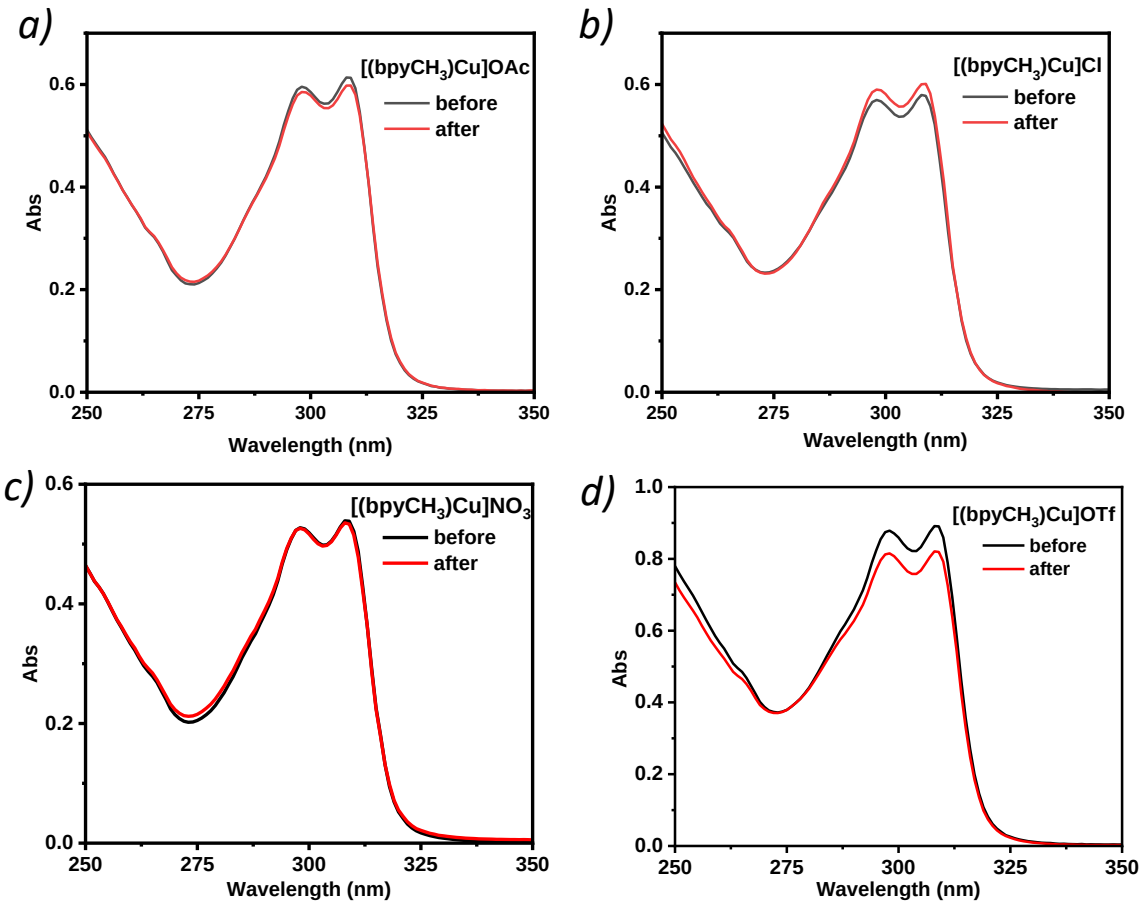

Figure S54. UV-Vis of [(bpyCH$_3$)Cu]X before and after the CPE experiment.

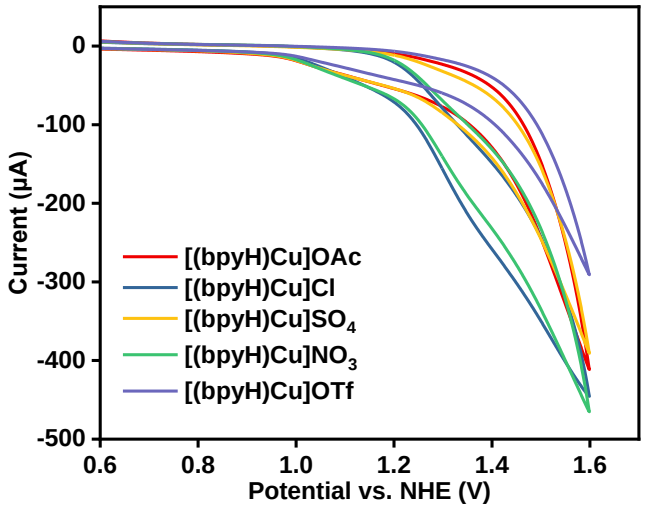

Figure S55. CV of the glassy carbon surface after the CPE experiment for [(bpyH)Cu]X.

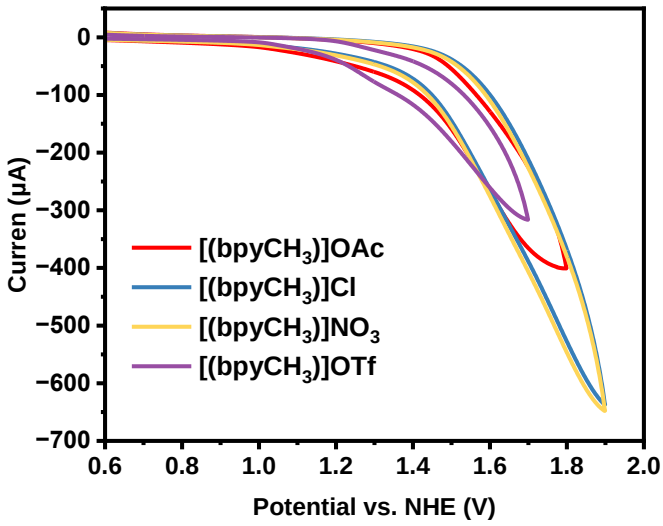

Figure S56. CV of the glassy carbon surface after the CPE experiment for [(bpyCH$_3$)Cu]X.

Generated oxygen measurement on ITO electrode

To verify and quantify the electrochemical oxygen generation, control potential electrolysis (CPE) experiments were carried out at a potential of 1.60 V vs NHE, with a 1 cm ×1 cm ITO electrode in a 0.1 M NaOAc/NaOH solution at pH = 12.5. The amount of oxygen was determined by gas chromatography, and the Faradaic efficiency was calculated based on the total charge passing through.

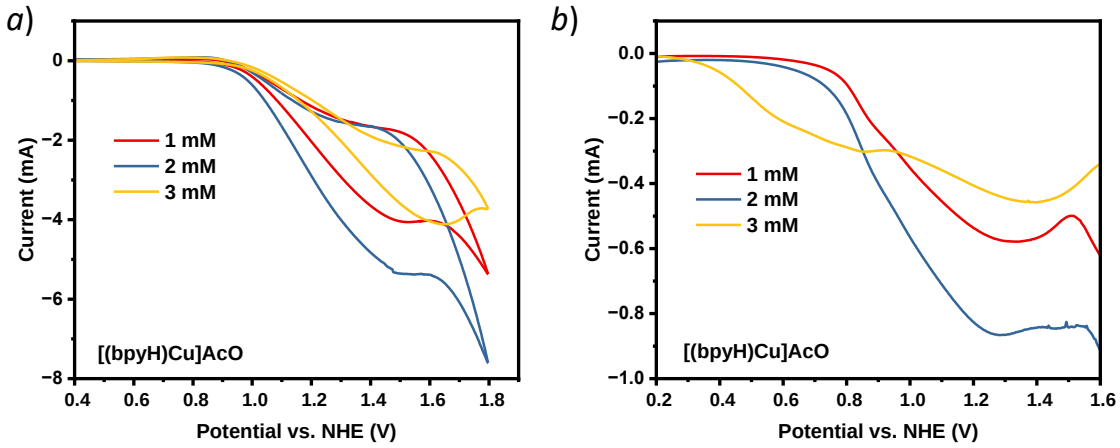

Figure S57. CVs and SWVs of [(bpy)HCu]OAc with different concentrations of the complex at pH 12.5 in 0.1M NaOAc/0.1 M NaOH.

Discussion: Figure S57 shows that the 2 mM catalyst has the highest current under the same conditions, hence the following measurements were taken at 2 mM of catalysts.

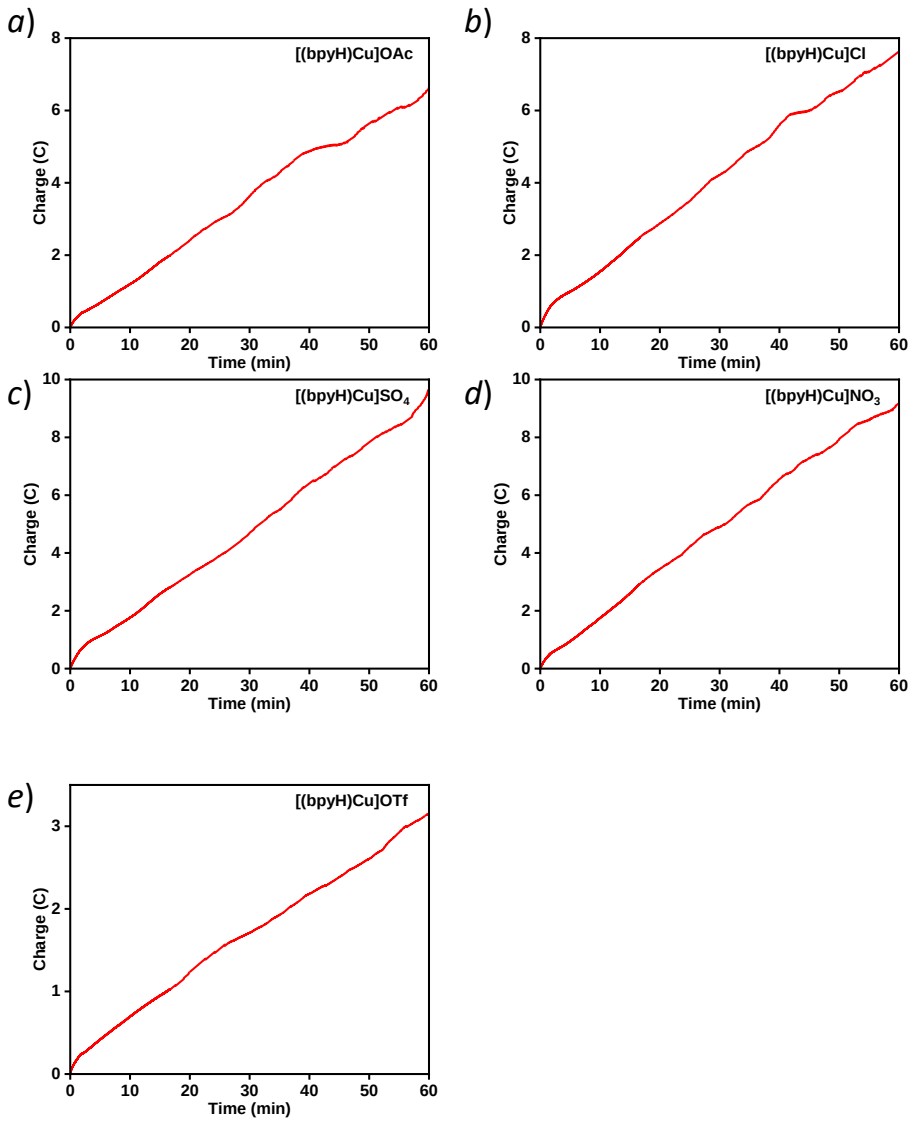

Figure S58. Control potential electrolysis of a solution containing 2 mM catalyst on an ITO electrode (S = 1 cm^2).

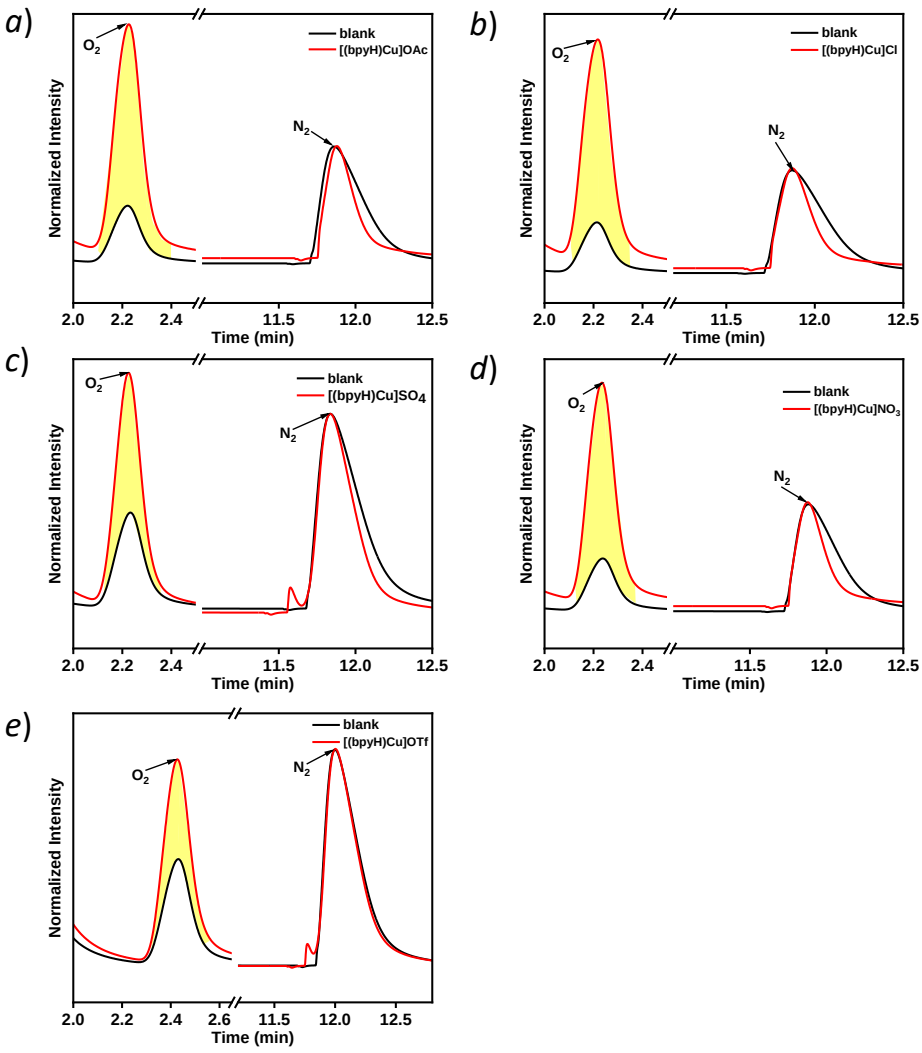

Figure S59. GC traces from a representative CPE experiment. The black line shows the air background. Oxygen amount is determined by comparing the relative intensity of oxygen and nitrogen, as shown in the yellow area.

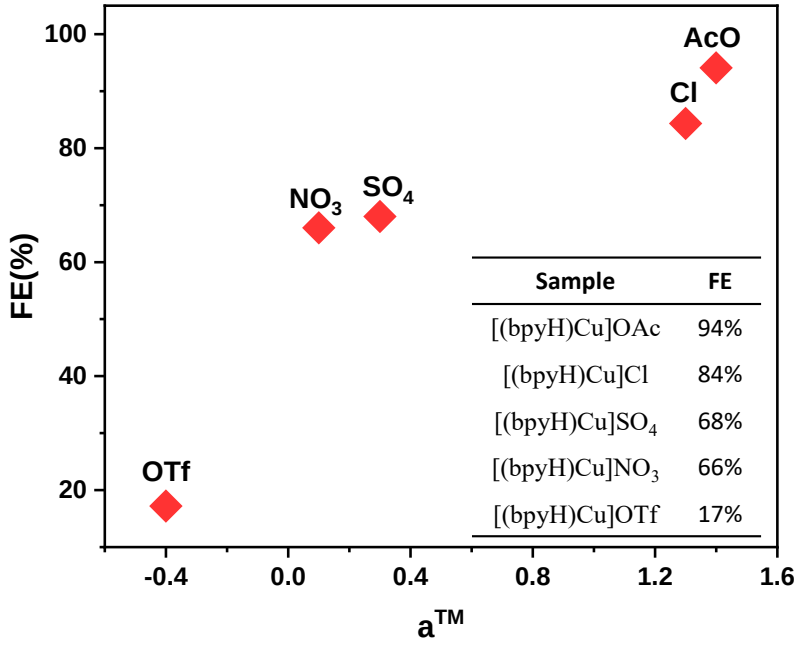

Figure S60. The relationship between Faradaic efficiency and a^{TM}.

References

1. Barnett, S. M.; Goldberg, K. I.; Mayer, J. M., A soluble copper–bipyridine water-oxidation electrocatalyst. *Nat. Chem.* **2012,** *4* (6), 498-502.
2. Fabian, I., Hydrolytic reactions of copper (II) bipyridine complexes. *Inorg. Chem.* **1989,** *28* (20), 3805-3807.
3. Garribba, E.; Micera, G.; Sanna, D.; Strinna-Erre, L., The Cu (II)-2, 2′-bipyridine system revisited. *Inorg. Chim. Acta* **2000,** *299* (2), 253-261.
4. Juris, A.; Balzani, V.; Barigelletti, F.; Campagna, S.; Belser, P.; von Zelewsky, A., Ru(II) polypyridine complexes: photophysics, photochemistry, electrochemistry, and chemiluminescence. *Coord. Chem. Rev.* **1988,** *84*, 85-277.
5. Kolthoff, I.; Tomsicek, W. J., The oxidation potential of the system potassium ferrocyanide–potassium ferricyanide at various ionic strengths. *J. Phys. Chem. C* **2002,** *39* (7), 945-954.
6. Barnett, S. M.; Goldberg, K. I.; Mayer, J. M., A soluble copper–bipyridine water-oxidation electrocatalyst. *Nat. Chem.* **2012,** *4* (6), 498-502.
7. Saveant, J.; Vianello, E., Potential-sweep chronoamperometry: Kinetic currents for first-order chemical reaction parallel to electron-transfer process (catalytic currents). *Electrochimica Acta* **1965,** *10* (9), 905-920.
8. Yin, Q.; Xu, Z.; Lian, T.; Musaev, D. G.; Hill, C. L.; Geletii, Y. V., Tafel Slope Analyses for Homogeneous Catalytic Reactions. *Catalysts* **2021,** *11* (1), 87.
9. Costentin, C.; Drouet, S.; Robert, M.; Saveant, J. M., Turnover numbers, turnover frequencies, and overpotential in molecular catalysis of electrochemical reactions. Cyclic voltammetry and preparative-scale electrolysis. *J. Am. Chem. Soc.* **2012,** *134* (27), 11235-11242.
10. Anantharaj, S.; Karthik, P. E.; Noda, S. J. A. C. I. E., The significance of properly reporting turnover frequency in electrocatalysis research. *Angew. Chem.* **2021,** *60* (43), 23051-23067.
11. Delley, B., From molecules to solids with the $DMol^3$ approach. *J. Chem. Phys.* **2000,** *113* (18), 7756-7764.
12. Delley, B., Hardness conserving semilocal pseudopotentials. *Phys. Rev. B* **2002,** *66* (15), 155125.
13. Perdew, J. P.; Burke, K.; Ernzerhof, M., Generalized gradient approximation made simple. *Phys. Rev. Lett.* **1996,** *77* (18), 3865.